Biomaterials Advances 154 (2023) 213613

Contents lists available at ScienceDirect

Biomaterials Advances

journal homepage: www.journals.elsevier.com/materials-science-and-engineering-c

Antibacterial and bioactive multilayer electrospun wound dressings based on hyaluronic acid and lactose-modified chitosan

Martina Gruppuso [a,1], Gianluca Turco [a], Eleonora Marsich [b], Davide Porrelli [a,*,2]

[a] Department of Medicine, Surgery and Health Sciences, University of Trieste, Piazza dell'Ospitale 1, 34129 Trieste, Italy
[b] Department of Medicine, Surgery and Health Sciences, University of Trieste, Via Licio Giorgieri 5, 34127 Trieste, Italy

ARTICLE INFO

Keywords:
Electrospinning
Chronic wounds
Multilayer
Hyaluronic acid
Lactose-modified chitosan
Rifampicin

ABSTRACT

Antibacterial multilayer electrospun matrices based on hyaluronic acid (HA) and a lactose-modified chitosan (CTL) were synthetized (i) by combining electrospun polycaprolactone (PCL) and polysaccharidic matrices in a bilayer device and (ii) by sequentially coating the PCL mat with CTL and HA. In both cases, the antibacterial activity was provided by loading rifampicin within the PCL support. All matrices disclosed suitable morphology and physicochemical properties to be employed as wound dressings. Indeed, both the bilayer and coated fibers showed an optimal swelling capacity (3426 ± 492 % and 1435 ± 251 % after 7 days, respectively) and water vapor permeability (160 ± 0.78 g/m^{2}h and 170 ± 12 g/m^{2}h at 7 days, respectively). On the other hand, the polysaccharidic dressings were completely wettable in the presence of various types of fluids. Depending on the preparation method, a different release of both polysaccharides and rifampicin was detected, and the immediate polysaccharide dissolution from the bilayer structure impacted the antibiotic release (42 ± 4 % from the bilayer structure against 25 ± 2 % from the coated fibers in 4 h). All the multilayer matrices, regardless of their production strategy and composition, revealed optimal biocompatibility and bioactivity with human dermal fibroblasts, as the released bioactive polysaccharides induced a faster wound closure in the cell monolayer (100 % in 24 h) compared to the controls (78 ± 8 % for untreated cells and 89 ± 5 % for cells treated with PCL alone, after 24 h). The inhibitory and bactericidal effects of the rifampicin loaded matrices were assessed on *S. aureus*, *S. epidermidis*, *E. coli*, and *P. aeruginosa.* The antibacterial matrices were found to be highly effective except for *E. coli*, which was more resistant even at higher amounts of rifampicin, with a bacterial concentration of 6.4 ± 0.4 log CFU/mL and 6.8 ± 0.3 log CFU/mL after 4 h in the presence of the rifampicin-loaded bilayer and coated matrices, respectively.

1. Introduction

The employment of electrospun matrices for chronic wound care is widely studied for their ability to sustain and promote tissue remodeling and repair of skin defects [1,2]. For example, the nanofibrous architecture offers a suitable biomimicry of the extracellular matrix (ECM) structure, whilst the large surface area and porosity favor gas permeation, the drainage of fluids, and the maintenance of a moist environment, thereby promoting tissue regeneration and wound closure with an anti-scarring and hemostatic potential [3,4]. In addition, the electrospinning can be performed in the presence of a wide variety of both synthetic and natural polymers (namely, proteins and carbohydrate polymers), where the natural ones could be ECM constituents themselves, thereby offering both a structural and compositional biomimicry [5,6]. This is the case, for instance, of hyaluronic acid (HA), which is a high-molecular weight non-sulfated glycosaminoglycan made of a linear repetition of (β 1 → 4)-glucuronic acid and (β 1 → 3)-*N*-acetyl-D-glucosamine residues. It is abundant in the connective tissues of

Abbreviations: DCM, dichloromethane; DMF, *N*,*N*-dimethylformamide; DMSO, dimethyl sulfoxide; ECM, extracellular matrix; CTL, lactose-modified chitosan; HA, hyaluronic acid; PCL, poly (ε-caprolactone); PCL bilayer, double layer electrospun membranes; PCL coating, membranes coated with polysaccharides; PEO, polyethylene oxide; Rif bilayer, rifampicin-loaded double layer electrospun membranes; Rif coating, rifampicin-loaded membranes coated with polysaccharides; WVTR, water vapor transmission rate.

* Corresponding author at: Department of Life Sciences, University of Trieste, Via Alexander Fleming 31/B, 34127 Trieste, Italy.
E-mail addresses: martina.gruppuso@burlo.trieste.it (M. Gruppuso), gturco@units.it (G. Turco), emarsich@units.it (E. Marsich), dporrelli@units.it (D. Porrelli).
[1] Present address: Institute for Maternal and Child Health–IRCCS "Burlo Garofolo"–Trieste, Via dell'Istria 65, 34137 Trieste, Italy.
[2] Present address: Department of Life Sciences, University of Trieste, Via Alexander Fleming 31/B, 34127 Trieste, Italy.

https://doi.org/10.1016/j.bioadv.2023.213613
Received 1 March 2023; Received in revised form 11 August 2023; Accepted 26 August 2023
Available online 28 August 2023

mammals, as the extracellular matrix of the skin, where it exerts a lubricating effect and prevents the drying of the tissue [7,8]. Moreover, hyaluronic acid possesses anti-inflammatory and antioxidant properties, guides collagen fiber deposition and thus prevents scarring. It can be recognized by cells *via* the CD44 receptor, so it controls cell migration in the early process of granulation [9]. Even chitosan and its derivatives can be considered wound healing promoters, although they are not naturally present in the ECM [10]. Among the chitosan derivatives, CTL (1-deoxylactic-1-γ-L-chitosan) stands out for its solubility in water at neutral pH values, as it is obtained by reductive amination with lactose aldehydic groups [11]. Not considering the biocompatibility, biodegradability as well as the hemostatic and antimicrobial properties typical of chitosan [12], CTL has been widely studied for its bioactivity in the osteochondral field as well as for its anti-inflammatory properties towards human dermal fibroblasts [11,13,14].

However, the solution properties of polysaccharides (as viscosity, conductivity, or surface tension) affect their electrospinnability, requiring the association with synthetic polymers and surfactants [15]. In this regard, polyethylene oxide is an FDA-approved synthetic polymer frequently associated to water-soluble polysaccharides, due to its biocompatibility, inertness, and hydrophilicity along with its ability to promote polymer chain entanglement directing filament extrusion [16]. On the other hand, surfactants as Tween® 20 are essential to improve solution surface tension and conductivity, thus favoring the production of thin and defect-free fibers [17].

Unfortunately, polysaccharides also possess poor mechanical properties, thereby impairing matrix handleability and application to the wound bed. Mixing natural and synthetic polymers is the most common approach to improve not only the electrospinnability of polysaccharides, but also their mechanical stability [18]. However, even the production of multilayer electrospun matrices has been proven to be a valid technique to obtain mechanically stable and easy to handle nanofibrous wound dressings [19].

The multilayer structures can be obtained by layer-by-layer deposition of polysaccharidic coatings on a synthetic-based electrospun support, as they combine in an ease and effective way the mechanical stability of the synthetic fibrous and highly porous meshes with polysaccharide bioactivity and ability to interact with the surrounding wound microenvironment [20]. Otherwise, entirely electrospun bilayer structures have been synthetized, with the purpose to closely mimic ECM structure and composition: the synthetic portion of the scaffolds is thought to provide mechanical support and stability, whereas the polysaccharidic layer is functional to skin regeneration by maintaining proper wound bed hydration and rapidly delivering bioactive polymers to the damaged tissue [21].

As synthetic support, poly-ε-caprolactone (PCL) is one of the most used FDA-approved polymers, thanks to its biocompatibility and long-term stability, since it is slowly degraded in the physiological microenvironment upon ester bonds hydrolysis, while still retaining high mechanical strength with tensile properties comparable to the epithelial tissue [22–24].

It should also be considered that, together with the inclusion of polysaccharides, the multilayer structure also enables the functionalization of the device with additional bioactive moieties [25]; for instance, the bioactive polysaccharides could be complemented by antibacterial moieties able to eradicate infections already present at the wound site and to prevent at the same time the occurrence of new ones [26,27]. Among the broad-spectrum bactericidal antibiotics, rifampicin is known for its ability to impede bacterial protein synthesis by blocking the RNA-polymerase β subunits [28,29]. It is widely used in the tuberculosis treatment, but its activity against both Gram-negative and Gram-positive bacteria, as in the case of biofilm formation from staphylococci, should not be neglected [30,31]. For this reason, it has also been employed to treat wounds, which are commonly infected both from Gram-positive and Gram-negative bacteria [32,33].

Given these premises, the aim of this paper is to present two different types of polysaccharide-based multilayer matrices: (i) a fully electrospun device obtained by electrospinning a ternary mixture of HA/CTL/PEO on a PCL fibrous membrane; (ii) a coated mat obtained by layer-by-layer deposition of CTL and hyaluronic acid on an electrospun PCL substrate. Both types of multilayer matrices have been then endowed with antibacterial properties by introducing rifampicin in the PCL basal layer. The combined incorporation of hyaluronic acid and CTL within a nanofibrous mat represents a novelty in the wound care panorama, and the introduction of rifampicin offers a useful model to understand how such products could deliver antibacterial and, more in general, bioactive cues to the damaged site. Moreover, given the complexity of CTL electrospinning, the production of multilayer matrices through sequential electrospinning rather than with other production methods (as coaxial electrospinning) represents a favorable choice, since it allows a finer control of the process while ensuring proper handleability together with the incorporation of bioactive moieties.

2. Materials and methods

2.1. Materials

Hyaluronic acid (HA) (MW = 40–50 kDa; Batch N# 2018082984) and CTL hydrochloride (lactose-modified chitosan; Batch N# 350118) were provided by Sigea S.r.l. (Trieste, Italy) and BiopoLife S.R.L. (Trieste, Italy), respectively. CTL final composition, determined by ^{1}H NMR, was as follow: glucosamine residue 27 %, *N*-acetylglucosamine 18 %, and 2-(lactit-1-yl)-glucosamine 55 %; the calculated relative MW of CTL is around 1.5×10^{3} kDa, as determined by viscometry [34]. Polyethylene oxide (PEO) (MW = 900 kDa), poly (ε-caprolactone) (PCL) (MW = 80 kDa), Tween® 20, dichloromethane (DCM), *N*,*N*-dimethylformamide (DMF), dimethyl sulfoxide (DMSO), phosphate buffered saline (PBS), and the LB broth with agar were purchased from Sigma-Aldrich (Chemical Co. USA). Rifampicin (Rif) was acquired from EMD Millipore Corp. Fortuna Optima glass syringes (an inner diameter of 9 mm) were acquired from Sigma-Aldrich (USA). The D-ES30PN-20 W potential generator was purchased from Gamma High Voltage Research Inc. (Ormond Beach, FL, USA). The syringe pump, model KDS-100-CE, was acquired from KD Scientific (Holliston, MA, USA). Recombinant Trypsin−EDTA 1×, penicillin/streptomycin 100×, Fetal Bovine Serum (FBS), and Dulbecco's Modified Eagle Medium (DMEM) were purchased from Euroclone (Milan, Italy). Normal Human Dermal Fibroblasts, Fibroblast Growth Medium 2, and the Fibroblast Supplement Mix were acquired from PromoCell GmbH.

2.2. Membrane preparation

2.2.1. Bilayer electrospun membranes

The bilayered electrospun wound dressings (hereafter named "PCL bilayer") were obtained by combining PCL and polysaccharide-based monolayer matrices. In detail, the PCL basal layer was synthetized as described by Porrelli and co-workers [35]. Briefly, 12 % (w/V) PCL was solubilized in DCM:DMF mixture (solvent ratio, 7:3; 70 % *v*/v DCM and 30 % v/v DMF. For 10 mL of solution, 120 mg of PCL were solved in a solvent mixture of 7 mL of DCM and 3 mL of DMF), by first dissolving PCL in DCM overnight (o/n), followed by the addition of DMF the day after. The membranes were produced with the following parameters: voltage, 17 kV; distance between the tip of the needle and the collector, 25 cm; flow rate, 0.6 mL/h; needle gauge, 27 G; time, 60 min; temperature, 23 °C; relative humidity, 50 %. The negative pole of the high voltage power supply was connected to the collector pin, with the positive pole being connected to the needle. To confer hydrophilicity to the obtained PCL membranes, they were then activated for 1 min by air-plasma treatment, using a PDC 32-G Plasma Cleaner (Harrick Plasma, Ithaca, USA) in low power mode (6.8 W), with a pressure of 0.1 mTorr. After that, they were mounted on the planar collector for the following electrospinning step. The polysaccharidic layer was produced from a

ternary mixture of hyaluronic acid [2 % (w/V)], CTL [1 % (w/V)], and PEO [2 % (w/V)], according to what previously reported by the authors [36]. In brief, the three polymers were dissolved o/n in water. Then, the pH of both hyaluronic acid and CTL was adjusted to 7.5, with the aim to avoid the formation of complexes between the positively charged CTL and the negatively charged hyaluronic acid. CTL was afterwards added to the PEO solution and stirred for 3 h; then, hyaluronic acid was also added to obtain the final ternary mixture. After 30 min of equilibration 1 % (V/V) Tween® 20 was added and the solution was stirred o/n at room temperature. After obtaining the polysaccharidic mixture, it was electrospun on the plasma-treated PCL mat with the following parameters: voltage, 30 kV; distance between the tip of the needle and the collector, 20 cm; flow rate, 1.2 mL/h; needle gauge, 23 G; time, 60 min; temperature, 23 °C; relative humidity, 50 %. The negative pole of the high voltage power supply was connected to the collector pin, with the positive pole being connected to the needle.

To confer antibacterial properties to the PCL bilayer membranes, the rifampicin was incorporated into the PCL basal layer, with a procedure similar to what reported elsewhere by the authors [37]. In detail rifampicin was solubilized in DMF, prior to the addition of DMF to the PCL in DCM solution with a final drug concentration of 0.1 % (w/V). The solution containing rifampicin was then electrospun following the same experimental set-up employed for the non-functionalized membranes. Once PCL/Rif membrane was produced, the bilayer was synthetized by activating for 1 min the Rif-loaded matrix by air-plasma treatment (as mentioned above) and electrospinning the polysaccharidic ternary mixture on the PCL/Rif mat, thus obtaining the "Rif bilayer" membrane. Considering light sensitivity of rifampicin, all the procedure was executed under dark conditions.

2.2.2. Coated electrospun membranes

To realize the coated electrospun wound dressings (hereinafter called "PCL coating") both CTL and hyaluronic acid were solubilized in deionized water at the final concentration of 0.6 % (w/V) and their pH was adjusted to 7.2–7.4. The coating was then realized on a 1 min-plasma treated PCL membrane (Section 2.2.1) by sequentially curing CTL and hyaluronic acid successively on the nanofibrous matrix, with a wash in deionized water and air drying after each layer deposition. The volume of the polysaccharides employed varied depending on the dimensions of the samples: (a) 50 μL in the case of 6-mm PCL disks (mean weight, 1.9 ± 0.7 mg); (b) 100 μL for 13-mm PCL disks (mean weight, 4.1 ± 1.1 mg); (c) 200 μL for 25-mm PCL disks (mean weight, 8.2 ± 2.3 mg) (d) 600 μL on 5 × 5-cm PCL samples (mean weight, 21.3 ± 2.5 mg).

To impart antibacterial properties even to the PCL coating membranes, the rifampicin was added again to the PCL layer followed by the 1-min activation as described above (Section 2.2.1), and polysaccharide coating. The rifampicin-loaded PCL coating matrices will be named "Rif coating" from now on.

2.3. Scanning Electron Microscope (SEM) analysis

Dried membrane samples were placed on aluminum stubs covered with a double-sided carbon tape and sputter-coated with gold using a Sputter Coater K550X (Emitech, Quorum Technologies Ltd., UK). The morphological analysis was therefore performed with a scanning electron microscope (Quanta 250 SEM, FEI, Oregon, USA) working in secondary electron detection mode. The working distance was set at 10 mm to obtain the appropriate magnifications, and the acceleration voltage was set between 20 and 30 kV. Fiber diameters were calculated using Fiji software [38], by randomly selecting 50 fibers on each sample. Similarly, the Fiji software was employed to estimate the porosity of the analyzed matrices.

2.4. Attenuated total reflectance – Fourier transform infrared (ATR-FTIR) spectroscopy

ATR-FTIR analysis was carried out on multilayer matrices to estimate the presence of both polysaccharides and rifampicin on the final products, by comparing them with the pure spectra of the single membrane components (namely, PCL, rifampicin, HA, CTL, PEO).

In all cases, IR spectra were recorded in transmittance mode with a Nicolet iS50 FT-IR spectrometer (Thermo Scientific, MI, Italy), within a wavenumber range of 4000–500 cm^{-1}. All the spectra were acquired with 32 scans and a resolution of 4 cm^{-1}.

2.5. X-ray powder diffraction (XRD) analysis

The crystallographic state of the rifampicin within the PCL layer was analyzed by X-ray Powder Diffraction at the Department of Mathematics and Geosciences of the University of Trieste, using a STOE D 500 X-ray diffractometer at room temperature. Three types of samples were studied: i) the pure antibiotic powder; ii) a control PCL membrane without antibiotic; iii) a PCL/Rif mesh. The CuKα radiation was used through a flat graphite crystal monochromator, with a current of 20 mA and a voltage of 40 kV. The 2θ scanning angle ranged from 2 to 30°, with 0.1° steps and a counting time of 2 s/step.

2.6. Swelling tests

The ability of the multilayer matrices to retain liquids was assessed after rehydration in PBS and measuring the changes of weight as a function of the immersion time. The PCL bilayer and PCL coating membranes were compared to the plasma-treated PCL mats, and 4 disks for each condition were analyzed (diameter, 25 mm; mean weight, 8.2 ± 2.3 mg). Once measured dry weights, wet weights were determined at each timepoint (1, 4, 24, 96, 168 h), by gentle blotting with a filter paper to remove the exceeding surface liquid.

The swelling ratio was then calculated according to Eq. (1):

$$\text{Swelling } (\%) = \left(\frac{(W_s - W_d)}{W_d}\right) \times 100 \quad (1)$$

where W_d and W_s are the weights of the samples in the dry and the swollen state, respectively.

2.7. Water vapor transmission rate (WVTR)

The water vapor permeability was assessed for both the PCL bilayer and PCL coating matrices, comparing them with the plasma-treated PCL mats.

Glass vials with a top closure of 13 mm of diameter were filled with deionized water, leaving a 2 cm gap between the water and the sample, which was placed as a cap on the top of the vial and sealed on the side with Parafilm®. The vials were then weighted and incubated at 37 °C for 24, 48, and 72 h, by measuring water loss at each timepoint. Uncapped vials and vials capped with Parafilm® were used as free evaporation and totally occlusive controls, respectively. The water vapor transmission rate was afterwards calculated using Eq. (2) [39]:

$$\text{WVTR}\left(\frac{g}{m^2 h}\right) = \left(\frac{(W_{tx} - W_{t0})}{A \times h}\right) \times 100 \quad (2)$$

where, W_{tx} is the weight after 24, 48, or 72 h, W_{t0} is the initial weight of the vial, and A is the area of the top closure of the vial. Three replicates were analyzed per each sample.

2.8. Contact angle and surface free energy analyses

The wettability of the multilayer matrices with and without rifampicin was assessed through contact angle measurement, using the sessile

drop method. Five samples (diameter, 6 mm; mean weight, 1.9 ± 0.7 mg) were analyzed for each condition, comparing untreated and plasma-treated PCL and PCL/Rif membranes. The contact angle was measured on images acquired with a stereomicroscope (Leica MZ16) equipped with a 45° tilted mirror and a digital camera (Leica DFC 320), then connected to the software Image Pro 3D Suite. Membrane wettability was studied in the presence of three types of fluids: (i) deionized water, (ii) deionized water +10 % FBS, (iii) FBS-supplemented DMEM. For each type of fluid, 4 μL were deposited on the sample and the images were acquired after 30 s of equilibration, to allow drop stabilization on the surface. The obtained images were thereafter analyzed using the "contact angle" tool of Fiji software and the contact angle of each kind of sample exposed to the various types of fluids was calculated. Surface free energies were subsequently evaluated using the Owens−Wendt method [40] adapted by Ren and co-workers [41] and Can-Herrera and co-workers [42]. Both deionized water and ethylene glycol (EG) contact angles (4 μL of fluid per sample) were examined to calculate the surface energy components, namely the polar/hydrophilic component (γ_s^p) and the dispersive/hydrophobic component (γ_s^d), respectively. The total surface free energy (γ_s) was, therefore, calculated according to Eq. (3):

$$\gamma_s = \gamma_s{}^p + \gamma_s{}^d \quad (3)$$

2.9. Polysaccharide release

The release of both CTL and hyaluronic acid from the PCL bilayer and PCL coating membranes was monitored in PBS after 1, 4, 24, 96, and 168 h, upon incubation at 37 °C in the dark. To this aim, fluorophore-conjugated polysaccharides, namely CTL-FITC and HA-CF640R (provided by prof. Ivan Donati, University of Trieste, Trieste, Italy) were employed; the polysaccharides were synthetized according to the procedures described by Sacco and co-workers [43] and Porrelli and co-workers [13]. The fluorescent matrices were prepared as described in Section 2.2.2, by substituting the non-fluorescent polysaccharides with the labeled ones. Once obtained the membranes, six disks (diameter, 13 mm; mean weight, 4.1 ± 1.1 mg) for each condition examined were placed in 24-wells culture plates, adding 1 mL of PBS in each well. At each timepoint, 200 μL of PBS were collected from each sample and transferred to a 96-well black plate for fluorescence reading (CTL-FITC excitation and emission wavelengths: 485 nm and 520 nm, respectively; HA-CF640R excitation and emission wavelengths: 642 nm and 662 nm, respectively) through a GloMax Multi+ Detection System (Promega corporation, Madison, USA). A calibration curve was used to relate the fluorescence intensity to the amount of CTL and hyaluronic acid released. The residual PBS was then removed from the wells and substituted with fresh medium, to evaluate polysaccharide cumulative release [44–46]. PCL electrospun samples were used as blanks.

2.10. Rifampicin release

The release of rifampicin from the Rif bilayer and Rif coating membranes was followed over time (1, 4, 24, 96, 168 h) by immersing them in PBS and incubating at 37 °C in dark conditions. Six disks (diameter, 13 mm; mean weight, 4.1 ± 1.1 mg) for each type of sample were placed in 24-wells culture plates, by adding 1 mL of PBS in each well. After each timepoint, 800 μL of release solution were collected from every sample and transferred to a quartz cuvette to evaluate the absorbance. The residual PBS was substituted with fresh medium, to evaluate antibiotic cumulative release [44–46]. The released rifampicin was quantified by means of UV spectrophotometry (Ultraspec 2100 pro, Amersham Bioscience) at 475 nm and the Lambert-Beer equation was exploited, by estimating through a calibration curve that ε_{475nm} is equal to 15,400. PCL electrospun samples were used as blanks.

To evaluate the influence of polysaccharides released from bilayer membranes on the release of the antibiotic, two disks (diameter, 13 mm) of PCL/Rif membranes were immersed in two different PBS solutions, enriched or not in CTL and hyaluronic acid (by estimating the amount of polysaccharide that would be released from a 13-mm PCL bilayer sample). After 1 h of immersion, the absorbance at 475 nm of the two solutions was measured, estimating the rifampicin concentration using the Lambert-Beer equation.

2.11. Cell culture

NIH-3 T3 murine fibroblasts (ATCC CRL-1658) were cultured in high-glucose DMEM supplemented with 10 % FBS, 2 mM L-glutamine, 100 U/mL penicillin, and 0.1 mg/mL streptomycin by maintaining them in humid atmosphere conditions, at 37 °C and with 5 % pCO_2. The cells were sub-cultured three times a week or at a confluence level of about 70–80 %.

Normal Human Dermal Fibroblasts (NHDF) from adult donor were cultured under humid atmosphere at 37 °C and with 5 % pCO_2 in their own Fibroblast Growth Medium 2, supplemented with 100 U/mL penicillin, 0.1 mg/mL streptomycin, and the related Fibroblast Growth Medium 2 Supplement Mix, which was stored in the dark. Cells were sub-cultured, using 0.25 % trypsin, when the confluence level was estimated at about 80 %. Cells at the second passage of culture were used for the biological tests.

2.11.1. Biocompatibility assay

Considering the potential cytotoxic effects of Tween® 20 employed for polysaccharide electrospinning, both PCL bilayer and Rif bilayer matrices were washed rapidly (2 min) in ethanol to remove the Tween® 20 surfactant from the electrospun matrices without affecting their integrity. To first evaluate the efficacy of the ethanol washing in improving mat biocompatibility, PCL bilayer membranes, washed with or without ethanol, were tested on NIH-3 T3 cells, by using cells grown in plain medium as control. Both types of membranes tested were cut in disks (diameter, 6 mm; mean weight, 1.9 ± 0.7 mg) and sterilized under UV irradiation for 45 min. After that, 20,000 cells/well suspended in 1 mL of complete DMEM were seeded onto 24-well culture plate, considering five replicates for each condition. The plates were then incubated at 37 °C with 5 % pCO_2 for 4 h to allow cell adhesion. After cell adhesion, two disks per sample type were placed on their respective wells and cell viability was assessed after 24 h using a Resazurin Cell Viability Assay kit (Sigma Aldrich, St. Louis). In detail, the cell culture medium was removed from the wells and replaced with 400 μL of Resazurin solution (diluted 1:30 in DMEM). After 4 h of incubation, 200 μL of the Resazurin solution were collected from each well and transferred to a 96-well black plate for fluorescence measurement, which was performed using a spectrofluorometer GloMax Multi+ Detection System (Promega corporation, Madison, USA), with an excitation wavelength of 525 nm and an emission wavelength in the range of 580–640 nm.

After assessing the efficacy of ethanol washing, the biocompatibility of all the multilayer matrices, loaded or not with rifampicin, was tested on NHDF. All types of membranes were cut in disks (diameter, 6 mm; mean weight, 1.9 ± 0.7 mg) and sterilized under UV irradiation for (i) 45 min in the case of the membranes without rifampicin, (ii) 10 min in the case of the antibiotic-enriched mats. Cells were suspended at a density of 20,000 cells/well in 500 μL of complete Fibroblast Growth Medium and seeded onto 24-well cell culture plates, considering five replicates for each condition. The cell culture plates were thereafter incubated at 37 °C with 5 % pCO_2 for 4 h, to ensure cell adhesion on the bottom of the wells. Subsequently, two disks per type of sample were added to the corresponding cell-containing well, to assess cell viability in the presence of the material. Cells seeded in the absence of the material and treated with PCL and PCL/Rif mats were used as controls, while empty wells with the culture medium only and with the culture medium treated with the different types of matrices to test were used as blank samples. Cell proliferation was evaluated after 24, 48, and 72 h using the Resazurin Cell Viability Assay kit (Sigma Aldrich, St. Louis). At each timepoint, medium was removed from the wells and replaced with

400 μL of Resazurin solution (diluted 1:30 in the NHDF culture medium). After 4 h of incubation, 200 μL of the Resazurin solution were collected from each well and transferred to a 96-well black plate for fluorescence measurement. Meanwhile, each well was washed with PBS and replaced with 500 μL of fresh cell culture medium. The fluorescence was measured again through a spectrofluorometer GloMax Multi+ Detection System (Promega corporation, Madison, USA), with an excitation wavelength of 525 nm and an emission wavelength in the range of 580–640 nm.

2.11.2. Wound healing assay

The wound healing assay (also referred to as "scratch test") was performed to study *in vitro* the ability of the CTL and hyaluronic acid released from the PCL bilayer and PCL coating matrices to promote wound closure. To this aim, liquid extracts of the membranes were prepared. Specifically, 5 × 5 cm (mean weight, 21.3 ± 2.5 mg) electrospun membranes (PCL, PCL bilayer, and PCL coating) were sterilized under UV irradiation for 45 min and immersed in 10 mL of NHDF culture medium for 72 h. The PCL bilayer mats had been previously washed with ethanol (Section 2.11.1). The membranes were then removed from the medium, which was stored at 4 °C in the dark. NHDFs were seeded on 6-well cell culture plates (two replicates for each condition) at a density of 250,000 cells/well and incubated o/n at 37 °C to allow cell adhesion. The day after, the culture medium was removed from each well and 3 mL of liquid extract of the membranes were added to the cells. Cells treated with plain culture medium were used as controls. After 24 h, when cells reached at least 80 % of confluency, the medium was removed from each well, stored in a sterile Falcon tube, and replaced with PBS. A scratch was realized in each well using a 200 μL pipette tip, by gently impressing a first vertical scratch followed by a second scratch perpendicular to the first one. After the scratch was performed on the cell monolayer, PBS was removed and replaced with the previously stored conditioned medium. The scratch closure was followed over time through an optical microscope (Optech IB3 ICS) equipped with a Nikon D5200; 4 gaps were analyzed in each well, with a total of 8 repetition for each condition. The images were captured at different timepoints (t_0, 2, 4, 6, 10, 24, 48 h). The analysis was performed using the software ImageJ: the region of interest (ROI) was outlined per each scratch and the percentage of closure over time was plotted. For each sample, eight images were analyzed. The percentage of closure over time was calculated by relating the gap area at the defined timepoint to the gap area at t_0, thereby obtaining the percentage of closed area. The gap closure in time was then measured according to Eq. (4):

$$\text{Gap closure } (\%) = 100\% - \%\text{closed area} \quad (4)$$

2.12. Antibacterial tests

*Escherichia coli*ATCC 8739 (hereinafter called *Escherichia coli1*), *Escherichia coli* ATCC 25922 (hereinafter named *Escherichia coli2*), *Pseudomonas aeruginosa* (ATCC 27853), *Staphylococcus aureus* (ATCC 25923), and *Staphylococcus epidermidis* (ATCC 12228) were swiped on LB agar plates from a glycerol stock and grown o/n at 37 °C. For liquid culture, some bacterial colonies were collected from the Petri plates and resuspended in 5 mL of LB medium. Each bacterial inoculum was then incubated o/n at 37 °C under shaking conditions (140 rpm). The bacterial concentration was determined upon optical density measurements (Ultraspec 2100 pro, Amersham Bioscience) at 600 nm (OD_{600nm}).

2.12.1. Growth inhibition assay

The growth inhibition assay was carried out to evaluate the ability of the multilayer matrices loaded with rifampicin to inhibit bacterial growth even in a highly diluted environment, such as an exudating wound. To this aim, liquid extracts of the membranes (both Rif bilayer and Rif coating) were prepared by embedding 13-mm disks (mean weight, 4.1 ± 1.1 mg) in PBS. In both cases an initial antibiotic concentration of about 10 μg/mL was estimated through UV spectrophotometry measurements (Ultraspec 2100 pro, Amersham Bioscience) at 475 nm using the Lambert-Beer equation ($\varepsilon_{475nm} = 15{,}400$). In a 96-well plate serial 1:2 dilutions of membrane extracts in LB medium were performed from an initial concentration of 5 μg/mL to a final concentration of 0.3125 μg/mL. The test was performed in duplicate for each type of sample (Rif bilayer and Rif coating) in the presence of each bacterial strain (*Escherichia coli1*, *Pseudomonas aeruginosa*, *Staphylococcus aureus*, *Staphylococcus epidermidis*). In detail, 100 μL of bacteria at a density of 10^6 CFU/mL were added to each dilution; bacteria in LB medium only and exposed to membranes without antibiotic were used as growth control, whereas the medium without bacteria was selected as negative growth control. Subsequently, the 96-wells were placed in a plate reader at 37 °C (FLUOStar® Omega-BMG Labtech spectrophotometer) and the absorbance at 600 nm was measured for 20 h (with 30 min intervals between each measure).

To assess the sensitivity of the tested bacterial strains they were exposed to free rifampicin (previously dissolved in DMSO) at different concentrations (from 40 μg/mL to 0.16 μg/mL) and incubated at 37 °C for 18 h. After that, the bacterial growth was evaluated by spectroscopy measurement at 600 nm, to determine the minimum inhibitory concentration (MIC) [47,48].

2.12.2. Time killing test

The time killing test was performed to evaluate the ability of the released rifampicin to even exert a bactericidal activity. To this aim, the bacteria were diluted at a final concentration of 10^7 CFU/mL. As t_0 control, bacteria were serially diluted in PBS from 10^{-1} to 10^{-4} and 50 μL of every dilution were spread on a LB agar plate and incubated at 37 °C o/n. The bacteria (10^7 CFU/mL) were incubated at 37 °C under agitation (140 rpm) in the presence of the multilayer matrices loaded with rifampicin. The corresponding material without antibiotic were used as growth control. Specifically, 1.5 mL of each bacterial strain (*Escherichia coli2*, *Pseudomonas aeruginosa*, *Staphylococcus aureus*, *Staphylococcus epidermidis*) were cultured in the presence of three disks (diameter, 13 mm; mean weight, 4.1 ± 1.1 mg) of each type of membrane (Rif bilayer, PCL bilayer, Rif coating, PCL coating). At selected timepoints (30 min, 2 h, 4 h), 100 μL of each sample were serially diluted in PBS. 50 μL of each dilution were then spread on LB agar plates, which were incubated o/n at 37 °C. The day after, the colonies were counted and the CFUs/mL per each timepoint were calculated.

2.13. Statistical analyses

Statistical analyses were performed thanks to GraphPad software (Graphpad Holdings, LLC). Data not satisfying normality assumptions (Shapiro-Wilk test) were analyzed by means of Kruskal-Wallis and Mann–Whitney non-parametric tests for two groups comparison, applying Bonferroni's correction. On the other hand, data that satisfied the normality assumption were analyzed with ANOVA test, applying Bonferroni's correction. Statistical significance was pre-set at $\alpha = 0.05$.

3. Results

3.1. Bilayered and coated matrices

Two types of multilayer systems were synthetized: (i) an entirely electrospun matrix (hereinafter referred to as "PCL bilayer"), obtained by electrospinning a polysaccharidic solution based on hyaluronic acid and CTL on a synthetic PCL counterpart; (ii) a PCL membrane functionalized with polysaccharides (from now on called "PCL coating") realized by layer-by-layer deposition of CTL and hyaluronic acid on a PCL electrospun matrix. The same plasma-treated PCL basal layer (Fig. 1A) was chosen in both cases, because it was easy to manufacture and had good morphology with uniform and defect-free fibers, which have been previously characterized elsewhere by the authors even in

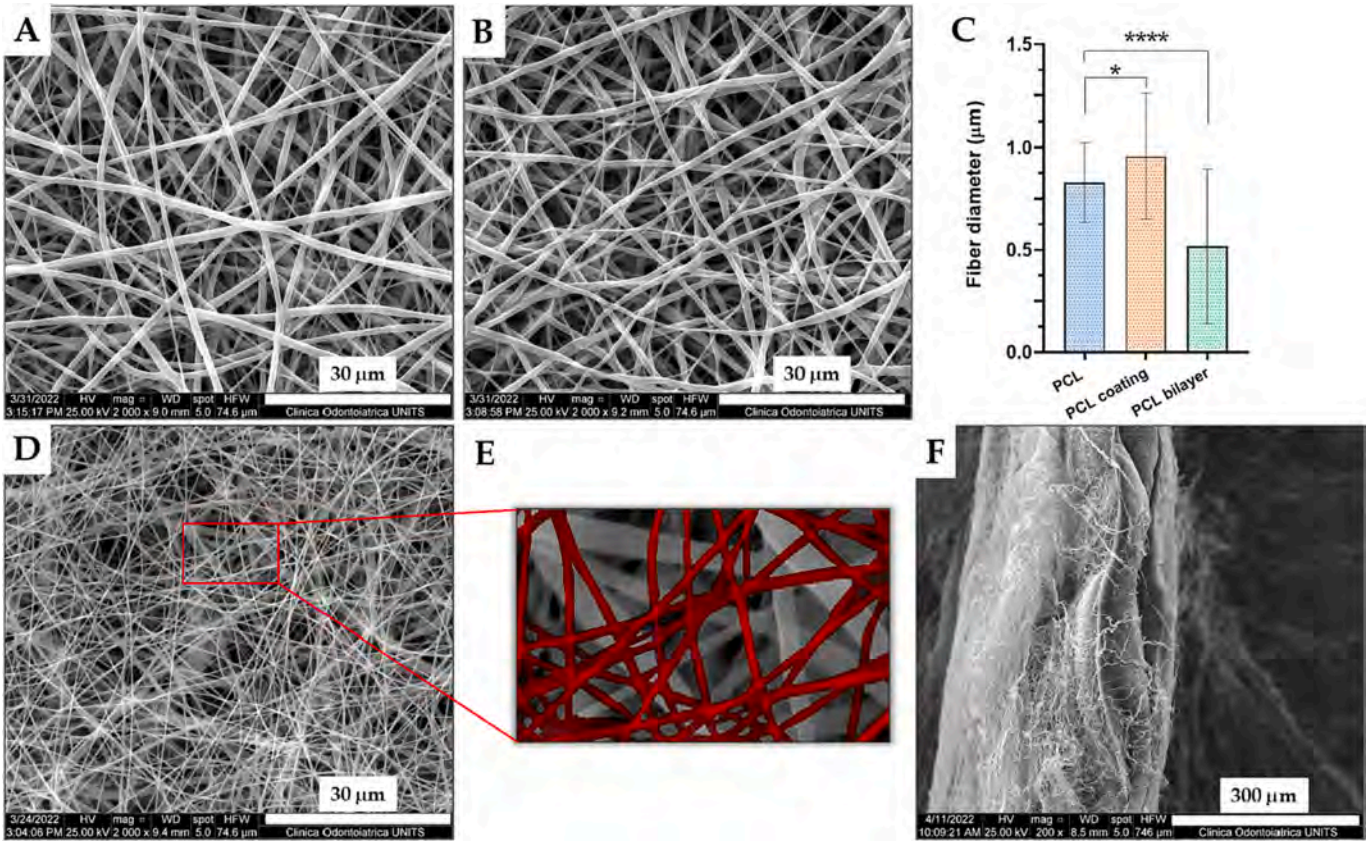

Fig. 1. Membranes microscopic aspect. SEM micrographs of a (A) plasma-treated PCL membrane and of multilayer matrices, namely (B) PCL coating and PCL bilayer in (D) front view with its magnification (E) and (F) cross section. In Fig. E, the dimensional analysis of the PCL and multilayer systems is reported. Statistical analysis was performed with Kruskal-Wallis test and Mann–Whitney test for two-groups comparison, applying Bonferroni's correction. Statistically significant differences are indicated as asterisks (*). **** = $p < 0.0001$. $N = 50$.

terms of mechanical performance [35]. In the case of the PCL coating mat (Fig. 1B) homogeneous and randomly oriented fibers without superficial defects were obtained, and the coating did not affect the goodness of the membrane.

The PCL bilayer system (Fig. 1D-F) showed, instead, the simultaneous presence of two uniform and superimposed electrospun matrices with (i) the thicker PCL fibers in the rear region and (ii) the thinner HA/CTL/PEO nanofibers in the front region (Fig. 1D-E). Moreover, by observing the matrix cross section, the two layers were clearly distinguishable (Fig. 1F). In Fig. 1C, the dimensional analysis of the plasma-treated PCL and of the multilayer matrices is reported.

A thorough dimensional analysis (reported in Fig. S1) revealed that the presence of the coating slightly altered the fiber diameter compared to the PCL alone, which is due to partial fiber rehydration. Meanwhile, the lower average fiber diameter calculated in the case of the PCL bilayer, which is associated to a higher standard deviation, could be due to the dual nature of the membrane: PCL fibers on one side and polysaccharide fibers on the other. Indeed, by analyzing the fiber diameter distribution in the three types of membranes, a homogenous distribution was observed in the case of PCL alone (Fig. S1A) and of the PCL coating (Fig. S1B), while the PCL bilayer showed a bimodal distribution of fiber diameter, which can be separated to highlight the two contributions given by the synthetic and polysaccharidic layers (Fig. S1C-E). The analysis of membrane porosity (Fig. S3) then revealed a reduction of the mean pore diameter in the presence of the PCL bilayer membranes (0.32 ± 0.25 μm) with respect to the other samples (0.50 ± 0.39 μm and 0.51 ± 0.37 μm in the case of the PCL and PCL coating mats, respectively), and this is probably due to the denser matrix formed by the upper polysaccharide-based nanofibrous layer.

3.1.1. *Rifampicin-loaded membranes*

In view of the compelling need for antibacterial wound dressings that can prevent and counteract bacterial infections at the wound site, the multilayer systems were enriched with an antibiotic agent, the rifampicin, thereby obtaining the so-called "Rif bilayer" and "Rif coating" membranes. The antibiotic was added directly to the PCL electrospinning solution and thus integrated into the fibrous PCL mesh, similar to what reported by Musciacchio and coworkers [49]. The resulting matrices (Fig. 2A-C) showed no significant morphological changes compared to the non-functionalized matrices, with the typical homogeneous, defect-free, and randomly oriented fibers. Likewise, both the dimensional (Fig. 2D, Fig. S2) and porosity analyses (Fig. S3) revealed similar results to the rifampicin-free mats. Even the statistical differences between the various types of membranes analyzed were comparable to those of the non-functionalized matrices, proving the goodness of the functionalization process, which does not alter the overall morphology.

3.2. *Physicochemical characterization*

3.2.1. *Membrane characterization by attenuated total reflectance – Fourier transform infrared (ATR-FTIR) spectroscopy (4000–500 cm^{-1})*

ATR-FTIR spectroscopy was exploited to evaluate the presence of polysaccharides and rifampicin on both the bilayer and coated matrices (Fig. 3). The spectra of all the membranes were compared to the spectra of their individual constituents. The presence of the polysaccharides was clearly detectable on the bilayer by the -OH band, which was even marked with respect to the polymers alone due to the combined effect of hyaluronic acid, CTL, and PEO. On the other side, the same band was less pronounced in the coated membranes, which can be attributed to

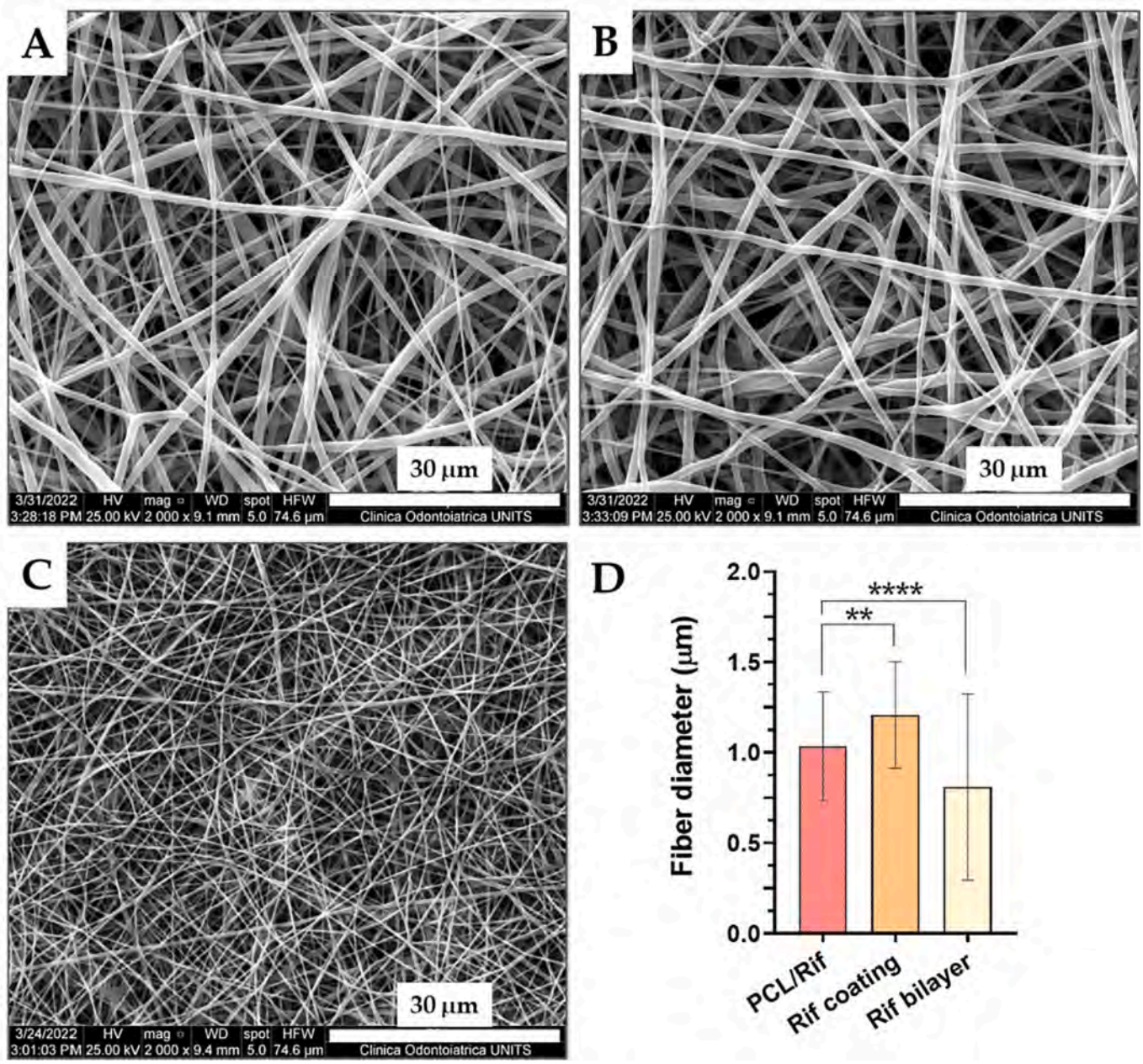

Fig. 2. Microscopic aspect of membranes loaded with rifampicin. SEM micrographs of rifampicin-loaded membranes, namely (A) PCL/Rif, (B) Rif coating, and (C) Rif bilayer. On the lower right, (D) the dimensional analysis. Statistical analysis was performed with Kruskal-Wallis test and Mann–Whitney test for two-groups comparison, applying Bonferroni's correction. Statistically significant differences are indicated as asterisks (*). **** = $p < 0.0001$. $N = 50$.

the lower concentration of the polysaccharides and to the absence of PEO, when compared to the bilayer. As regards the PCL support layer, it was detectable in the bilayer as well as in the coated matrices thanks to the -CH and C═O bands, while the rifampicin could not be distinguished in the final structure because its signal overlapped with that of the other polymers.

3.2.2. *Membrane characterization by X-ray powder diffraction (XRD)*

The crystallographic state of the rifampicin before and after its dissolution and incorporation into the PCL nanofibrous mesh was studied exploiting the X-ray Powder Diffraction analysis, with the purpose of identifying any changes in the antibiotic structure which could impact its biological performance. A PCL mat without antibiotic was used as comparison, as the PCL is known to be a semi-crystalline polymer [22]. The results (Fig. 4) confirmed the crystallinity of pure rifampicin powder, which revealed many characteristic peaks [50], the highest of which was observed for $2\theta = 19.8°$, given by the (212) plane. Even the PCL control membrane showed the semi-crystalline structure of the polymer, with its peaks at $2\theta = 21.3°$, $23.7°$ generated by the reflections of the (100) and (200) crystallographic planes [51]. On the other hand, in the case of the PCL/Rif mesh, only the two peaks of the PCL were clearly recognizable, whilst only a halo noise could be correlated to the rifampicin, effectively suggesting that the dissolution of the antibiotic before the electrospinning process induces a reorganization of the molecule, which loses is organized crystallinity moving into an amorphous state.

3.2.3. *Swelling behavior*

The liquid retention ability of the PCL bilayer and PCL coating mats was evaluated in PBS, as it is commonly employed to study the water

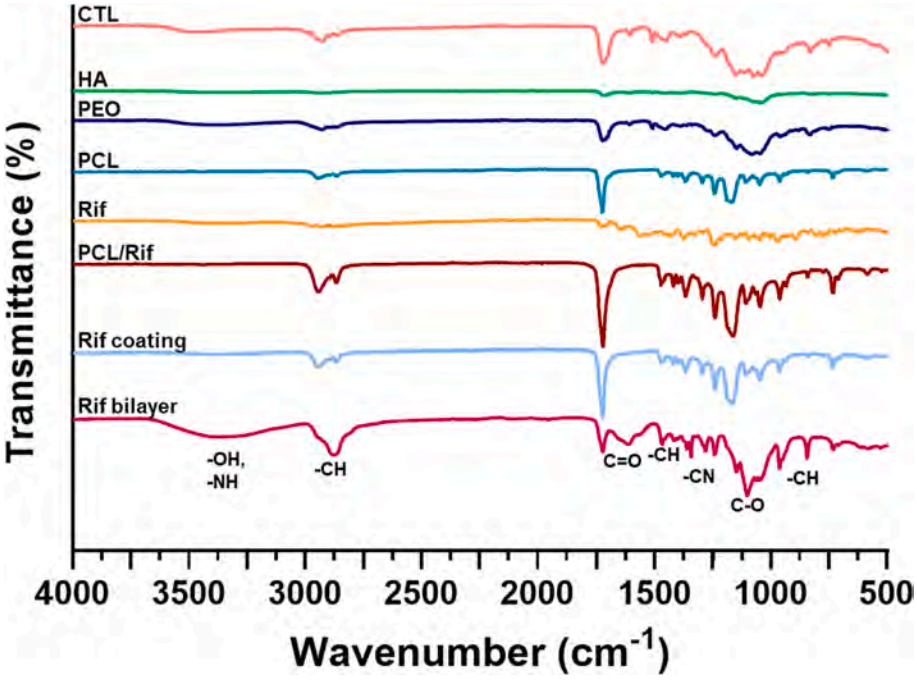

Fig. 3. Chemical characterization of membranes. ATR-FTIR spectra of Rif coating and Rif bilayer meshes, compared with the spectra of the single membrane components (namely, CTL, HA, PEO, Rifampicin, PCL) and of the basal PCL/Rif mat.

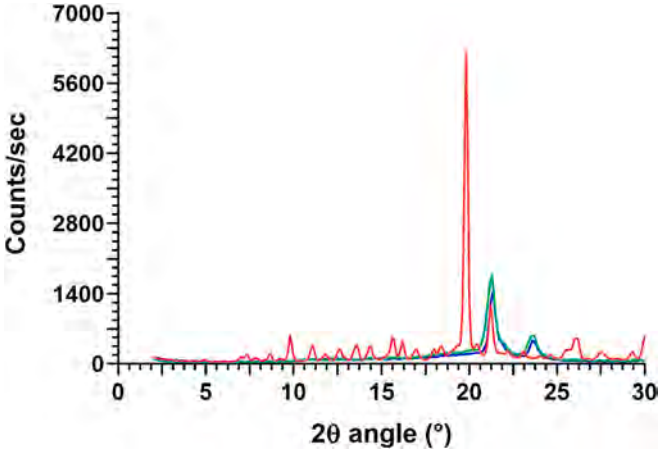

Fig. 4. Characterization of the crystallographic state of the rifampicin loaded matrices. XRD spectra of pure rifampicin powder (in red) compared with PCL (in green) and PCL/Rif (in blue) membranes.

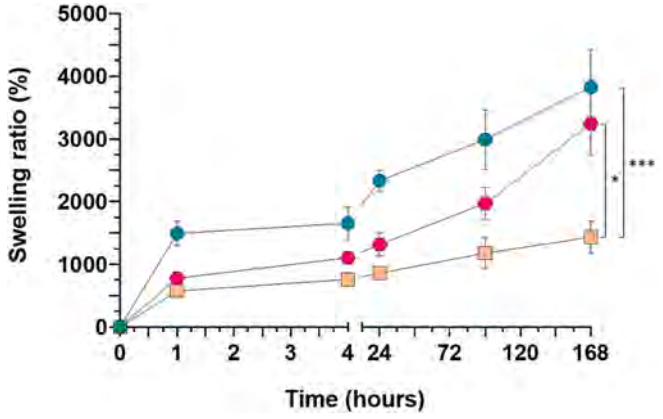

Fig. 5. Membrane swelling behavior. Swelling capacity in PBS of the PCL bilayer (●) and PCL coating (■) matrices, and of plasma-treated PCL mats (●). The statistical analysis was performed with ANOVA test, applying Bonferroni's correction. Statistically significant differences are indicated with asterisks (*). *** = $p < 0.0001$. $N = 4$.

uptake capacity of wound dressing devices [52–56].

The polysaccharide-based matrices were compared with the PCL alone, and their water uptake capacity was followed from 1 h up to 7 days. As can be observed in Fig. 5, the swelling behavior of the PCL bilayer mats was comparable to that of the pure plasma-treated PCL meshes, with a swelling ratio of about 4000 % after 7 days. On the other hand, albeit still considerable (about 1500 %), the PCL coating membranes showed a significant lower ability to absorb fluids, probably because the PCL porosity is partially masked by the rapid hydration of the overlying coating.

3.2.4. Membrane permeability

Water vapor permeability and, thus, the ability to promote gas exchanges was assessed up to 72 h in the presence of PCL bilayer and PCL coating mats, using plasma-treated PCL membranes as control. Parafilm® was used as non-permeability control, while unsealed vials were tested as control for total evaporation. The results (Fig. 6, Table S1) showed the optimal ability of all types of the tested membranes to transmit water vapor, with an evaporation efficiency halfway between total evaporation and lack of permeability. Moreover, this behavior was sustained until 72 h, revealing the effectiveness of these electrospun devices in maintaining an adequate moist environment at the wound site.

3.2.5. Membrane wettability and surface free energy

The wettability of PCL, PCL coating, and PCL bilayer matrices was examined using contact angle measurements. The samples with rifampicin were also analyzed, to study the influence of the antibiotic on the membrane surface properties. In the case of PCL alone, both untreated and plasma-treated mats were tested to examine the effectiveness of air-plasma treatment in increasing the hydrophilicity of the membranes.

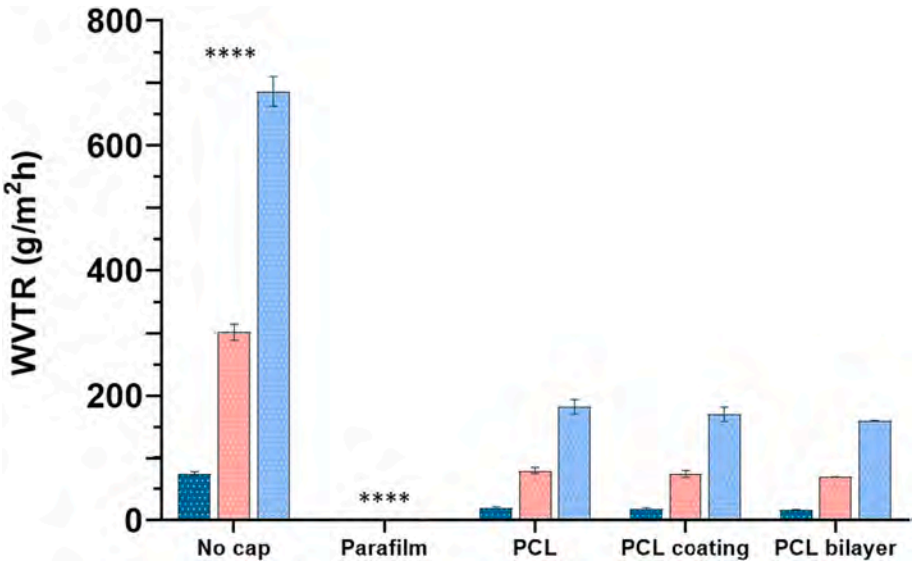

Fig. 6. Membranes permeability characterization. Water vapor transmission ability of plasma-treated PCL mats and of polysaccharide-enriched multilayer matrices (PCL coating and PCL bilayer) at 24 h (dark blue), 48 h (pink) and 72 h (light light blue). The statistical analysis was performed with ANOVA test, applying Bonferroni's correction. Statistically significant differences are indicated with asterisks (*). **** = $p < 0.0001$. The differences between the time points for the same sample are all statistically significant and have not been reported for sake of clarity. $N = 3$.

The wettability measurements were performed in the presence of three types of fluids, namely (i) water, (ii) water added with 10 % fetal bovine serum (FBS), to evaluate any possible interaction with serum proteins, and (iii) Dulbecco's Modified Eagle Medium (DMEM) completed with FBS, to assess membrane behavior in an *in vitro* cellular environment.

The membranes without rifampicin (Fig. 7) revealed a highly hydrophilic behavior, with a complete fluid spreading on their surface in all cases. The exception was the untreated PCL, which proved to be non-wettable with all media tested, confirming the effects of air-plasma treatment on the hydrophilicity of the membranes.

A similar wetting behavior was observed with the rifampicin-loaded mats (Fig. 8), with a complete spreading of the drop on the surface of

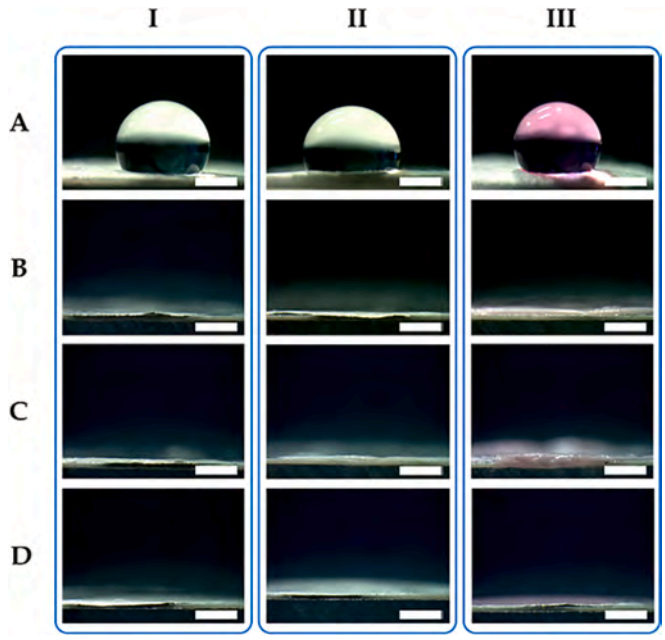

Fig. 7. Contact angle analysis. Images of the contact angle studied on (A) not-treated PCL, (B) plasma-treated PCL, (C) PCL coating, and (D) PCL bilayer matrices in the presence of (I) water, (II) water + FBS, and (III) DMEM. The absence of the drop is due to its complete spreading on the surface. Scale bar: 1 mm.

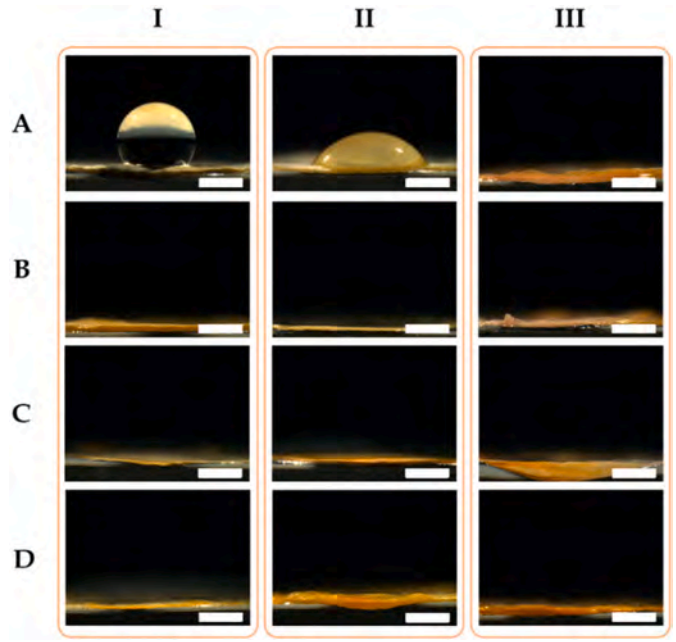

Fig. 8. Contact angle analysis. Images of the contact angle studied on Rif-loaded membranes: (A) not-treated PCL/Rif, (B) plasma-treated PCL/Rif, (C) Rif coating, and (D) Rif bilayer matrices in the presence of (I) water, (II) water + FBS, and (III) DMEM. The absence of the drop is due to its complete spreading on the surface. Scale bar: 1 mm.

both plasma-treated PCL/Rif and polysaccharide-enriched PCL/Rif mats. However, in the case of the non-activated PCL/Rif membranes, the expected hydrophobic behavior was retained in the presence of water and turned into a hydrophilic one in the case of water + FBS and DMEM. This can be attributed to the presence of rifampicin, which interacts with serum proteins and thereby increases the hydrophilicity of the membrane.

The surface free energy of the samples was, then, evaluated according to the Owens-Wendt method, by using the contact angle of water to calculate the polar/hydrophilic component (γ_s^p) and the contact angle of ethylene glycol to estimate the dispersive/hydrophobic

component (γ_s^d). The analysis was performed for both non-functionalized and rifampicin-loaded membranes (Table 1). In line with what observed in the wettability measurements, the high contact angle values of the non-activated PCL membranes (> 90°) together with the low values of the polar component (γ_s^p) confirmed their basically hydrophobic behavior. On the other hand, in the presence of rifampicin, the contact angles of untreated PCL membranes were < 90° for water + FBS and DMEM, leading to an increase of the polar component, evidence of the augmented hydrophilicity. In all other cases, contact angles equal to 0° were registered, with the polar component (γ_s^p) higher than not treated membranes, confirming membrane hydrophilicity.

3.2.6. Polysaccharide release

The stability of polysaccharides on the bilayer and coated PCL matrices was investigated, using a fluorescein-labeled CTL (CTL-FITC) and a CF640R-labeled hyaluronic acid (HA-CF640R) for membrane synthesis. The cumulative release of the labeled polysaccharides in PBS was followed from 1 h to 7 days by spectrofluorimetry. Not surprisingly, in the presence of the PCL bilayer, the polysaccharides were completely released after only 1 h. This can be explained by the high solubility of CTL and hyaluronic acid in aqueous environment, which is further enhanced by the large surface area of the electrospun products, making them even more available after immersion in water or aqueous solvents.

Conversely, the PCL coating membranes displayed a different behavior (Fig. 9). Indeed, the outer hyaluronic acid layer was almost completely released after 24 h (≈ 85 %), then the release kinetic stabilized and reached a plateau; meanwhile, the inner CTL layer was slowly released in the medium, with a release of ≈ 25 % after 24 h, then stabilizing also in this case. Such behavior could be attributed to the sequential coating procedure, with the CTL being directly retained by the underlying PCL nanofibrous mesh.

3.2.7. Rifampicin release

The cumulative release of rifampicin from the Rif bilayer and the Rif coating membranes was analyzed in PBS for 7 days by UV–visible spectroscopy and compared with the rifampicin release from plasma-treated and untreated PCL/Rif mats, to analyze the influence of the air-plasma activation on rifampicin integrity. The results (Fig. 10)

Table 1
Surface energy analysis. Mean values of the contact angle measurements and surface free energy components for not-functionalized and Rif-loaded membranes. The contact angle values of ethylene glycol were all equal to 0°. $N = 5$.

	Contact angle H_20 [deg]	Contact angle H_20 + FBS [10 %] [deg]	Contact angle DMEM [deg]	γ_s^d [mJ/m^2]	γ_s^p [mJ/m^2]	γ_s [mJ/m^2]
Not-treated PCL	124.9 ± 1.6	113.2 ± 2.5	119.5 ± 7.9	79.5 ± 0.1	13.3 ± 0.8	92.8 ± 0.8
Plasma-treated PCL	0.0 ± 0.1	0.0 ± 0.1	0.0 ± 0.1	79.5 ± 0.1	19.1 ± 0.1	98.5 ± 0.1
PCL coating	0.0 ± 0.1	0.0 ± 0.1	0.0 ± 0.1	79.5 ± 0.1	19.1 ± 0.1	98.5 ± 0.1
PCL bilayer	0.0 ± 0.1	0.0 ± 0.1	0.0 ± 0.1	79.5 ± 0.1	19.1 ± 0.1	98.5 ± 0.1
Not-treated PCL/Rif	126.0 ± 3.9	57.3 ± 4.5	0.0 ± 0.1	79.5 ± 0.1	13.9 ± 2.1	93.4 ± 2.1
Plasma-treated PCL/Rif	0.0 ± 0.1	0.0 ± 0.1	0.0 ± 0.1	79.5 ± 0.1	19.1 ± 0.1	98.5 ± 0.1
Rif coating	0.0 ± 0.1	0.0 ± 0.1	0.0 ± 0.1	79.5 ± 0.1	19.1 ± 0.1	98.5 ± 0.1
Rif bilayer	0.0 ± 0.1	0.0 ± 0.1	0.0 ± 0.1	79.5 ± 0.1	19.1 ± 0.1	98.5 ± 0.1

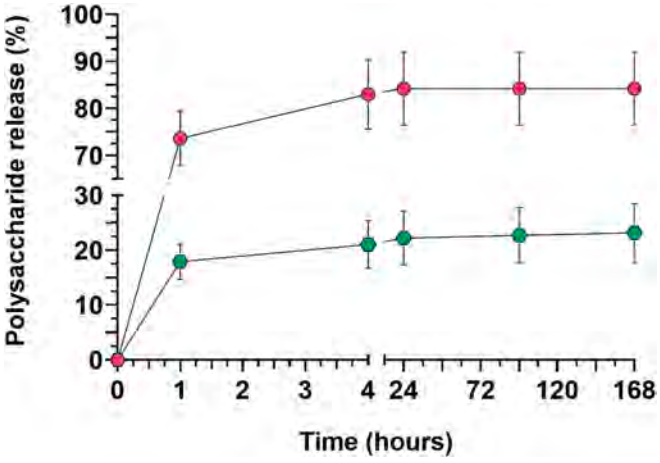

Fig. 9. Release of polysaccharides. Cumulative release of polysaccharides from PCL coating membranes expressed as percentage of CTL-FITC (●) and HA-CF640R (●) found in the PBS medium. $N = 6$.

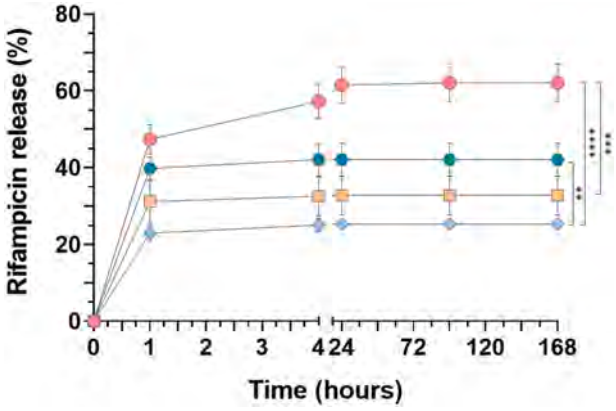

Fig. 10. Rifampicin release. Cumulative rifampicin release in PBS from non-activated (●) and plasma-treated PCL/Rif mats (■), Rif bilayer (●), and Rif coating (◆) electrospun matrices. The statistical analysis was performed with ANOVA test, applying Bonferroni's correction. Statistically significant differences are indicated with asterisks (*). **** = $p < 0.0001$. $N = 6$.

showed a significantly higher antibiotic release in the non-activated PCL/Rif membranes, which reached a plateau after 24 h. This is likely due to a lower amount of intact rifampicin within the nanofibrous mesh after the activation process, as this type of treatment appears to partially degrade the antibiotic, resulting in a significantly lower detectable release. Meanwhile, in the case of the plasma-treated mats, the antibiotic release was almost at its maximum after 4 h, then reaching a plateau, but a significant difference was observed between the Rif bilayer and Rif coating meshes. Despite the identical PCL/Rif base layer, the variation in the antibiotic release can be attributed to the different preparation method used to add CTL and hyaluronic acid to the PCL matrix. Indeed, in the case of Rif coating, the antibiotic loaded in the PCL mesh is partially solubilized during the layer-by-layer deposition and is trapped in the CTL layer, so it follows the slower polysaccharide release. On the other hand, in the case of Rif bilayer, the polysaccharides are immediately solubilized and readily available in the medium, thus moving the antibiotic release equilibrium towards the medium. This has been demonstrated by immersing two identical PCL/Rif membranes in two different media (namely, PBS and PBS enriched with polysaccharides) and evaluating the differential antibiotic release in the two. In the first case, 1.96 μg/mL of rifampicin were released, while in the presence of the polysaccharides the antibiotic release was of 2.59 μg/mL, revealing how the polysaccharides present in the medium impact on

the release equilibrium.

3.3. Biological characterization

3.3.1. Membrane biocompatibility

The biocompatibility of the PCL bilayer membranes was first tested on the murine cell line NIH-3 T3, to evaluate the potential cytotoxic effect of the Tween® 20 employed for their synthesis. For this reason, the PCL bilayer matrices were washed in ethanol for 2 min to extract the residual surfactant from the polysaccharidic layer, without affecting polysaccharide availability. As can be seen in Fig. 11A, the cells exposed to the PCL bilayer after 24 h suffered from the release of Tween® 20, while, after washing with ethanol, they showed comparable viability to the untreated controls. Once the efficacy of this post-processing step was established, the biocompatibility of all types of matrices (namely control PCL, PCL coating, and PCL bilayer with or without rifampicin) was studied using human dermal fibroblasts (HDF). The results (Fig. 11B) showed that all the tested nanofibrous structures were biocompatible, regardless of the preparation method and of the presence of the antibiotic.

3.3.2. Membrane bioactivity

A wound healing assay on human dermal fibroblasts was performed to test the bioactivity of the hyaluronic acid and CTL released both from the PCL bilayer and PCL coating matrices. Basically, a scratch was induced on a cell monolayer, and then cell migration and proliferation in time were followed until gap closure [57,58]. Untreated and PCL-treated cells were used as controls. As it can be seen from both the graph (Fig. 12A) and the images of the gap closure overtime (Fig. 12B-E and Figs. S4–5), the gap closes faster already at earlier time points (2 h) in the presence of the polysaccharide-endowed matrices, and this difference is even more visible at longer times (6–10 h).

Even after 24 h (Fig. 9B-E) a scratch is still clearly visible in the controls, whereas it is completely closed in the case of PCL coating and PCL bilayer membranes. After 48 h, the wound was finally closed in the controls. On the other hand, despite the slight difference between the PCL bilayer and the PCL coating mats, no significant difference was detected between the two. Considering the different release of polysaccharides between the two types of matrices, this behavior suggests that the burst release of hyaluronic acid from the PCL coating mesh in combination with even lower amounts of CTL is sufficient to exert a bioactive effect, thus inducing wound closure.

3.4. Microbiological characterization

3.4.1. Bacterial growth inhibition

The ability of the antibiotic released from the Rif bilayer and Rif coating membranes to inhibit the growth of bacteria was assessed using four bacterial strains that commonly infect the wound site: the Gram-negative strains *Escherichia coli* and *Pseudomonas aeruginosa* and the Gram-positive strains *Staphylococcus aureus* and *Staphylococcus epidermidis*. To test the inhibitory activity of rifampicin, liquid extracts of the membranes were prepared, and the bacteria were exposed for 20 h to different antibiotic concentrations, ranging from 5 μg/mL to 0.3125 μg/mL. The results (Fig. 13) revealed an optimal inhibitory effect of the rifampicin released from the fibrous mats (both bilayer and coated matrices) in the case of the Gram-positive bacteria, being active even at low concentrations. Similar results were obtained against the Gram-negative *Pseudomonas aeruginosa*. Unfortunately, the sensitivity of *Escherichia coli* strain to the tested concentrations of rifampicin was not as high as that of the other bacteria analyzed. At the highest concentration tested (5 μg/mL), the inhibitory effect was only slight after 5 h. Therefore, to assess the actual sensitivity of the bacterial strains analyzed, they were treated with free rifampicin at several concentrations (from 40 μg/mL to 0.16 μg/mL) and the bacterial growth was evaluated after 18 h upon spectroscopy measurements. The following minimum inhibitory concentrations (MICs) were obtained: 40 μg/mL for *Escherichia coli*, 1.25 μg/mL for *Staphylococcus aureus*, 0.16 μg/mL for *Staphylococcus epidermidis*, 0.625 μg/mL for *Pseudomonas aeruginosa*. To further confirm the resistance of the *Escherichia coli* strain examined, another strain was tested, namely *Escherichia coli2* (ATCC 25922), revealing a MIC value of 5 μg/mL.

3.4.2. Time killing

The bactericidal effect of the rifampicin-loaded membranes was tested on the same bacterial strains examined in the growth inhibition assay, namely *Staphylococcus aureus, Staphylococcus epidermidis*, *Pseudomonas aeruginosa*, and the more sensitive *Escherichia coli2*. In this case, the bacteria were directly grown in the presence of the membranes using not-functionalized matrices as controls, and the ability of the antibiotic-

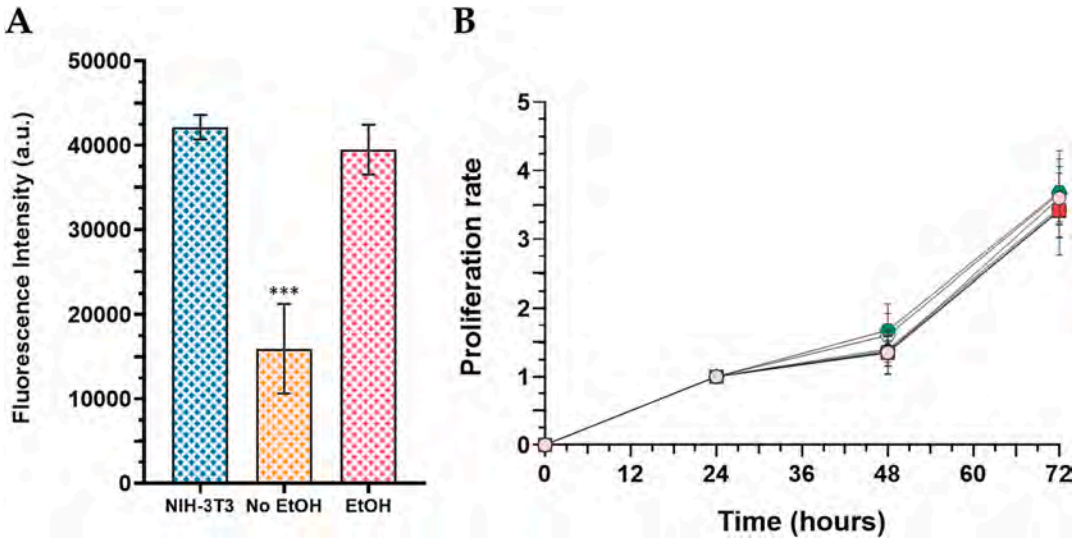

Fig. 11. Multilayer matrices biocompatibility studied through Alamar Blue Assay. (A) Evaluation of NIH-3 T3 cells viability in the presence of PCL bilayer membranes washed (EtOH) or not washed (No EtOH) with ethanol to extract Tween®20 residues. (B) Biocompatibility towards human dermal fibroblasts of PCL (■) and PCL/Rif (■), PCL coating (◆) and Rif coating (◆), PCL bilayer (●) and Rif bilayer (●) membranes. The control cells are indicated as pink circles (○). The statistical analysis was performed with ANOVA test, applying Bonferroni's correction. Statistically significant differences are indicated with asterisks (*). *** = $p < 0.001$. The differences between the time points in Fig. B are all statistically significant and have not been indicated for sake of clarity. $N = 5$.

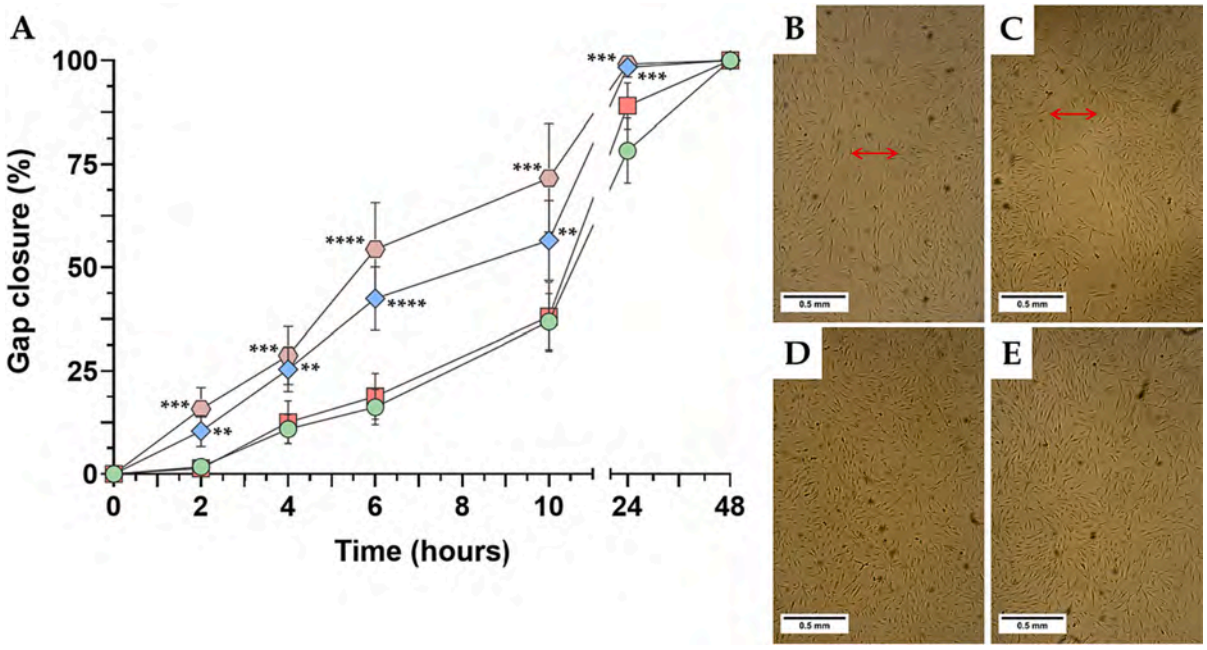

Fig. 12. Wound healing assay on human dermal fibroblast. On the left, (A) percentage of gap closure over time in the presence of the extracts from PCL bilayer (●) and from PCL coating (◆) membranes. The controls are represented by untreated cells (●) and cell treated with extract from polysaccharide-free PCL membranes (■). The statistical analysis was performed with ANOVA test, applying Bonferroni's correction. Statistically significant differences are indicated with asterisks (*). **** = $p < 0.0001$. $N = 8$. On the right, images of the cells after 24 h of treatment with (B) cell culture medium only, (C) PCL, (D) PCL coating, (E) PCL bilayer extracts. The red arrows indicate the extension of the gap persisting in the controls.

loaded membranes to kill the selected bacteria over time was assessed.

As can be seen in Fig. 14, the rifampicin-loaded mats exhibited a bactericidal effect on all strains tested, with *Staphylococcus epidermidis* being the most sensitive and *Escherichia coli* the most resistant. This was in line with what observed in the growth inhibition test, where the amount of rifampicin required to inhibit *Escherichia coli* growth was significantly higher than for the other bacterial strains.

4. Discussion

Looking at the advantages offered by multilayer nanofibrous wound dressings based on polysaccharides, which have been plenty discussed in the introduction, the current work proposes two types of multilayer mats: (i) a fully electrospun device obtained by electrospinning a ternary polysaccharidic mixture based on hyaluronic acid and CTL on a plasma-treated PCL electrospun membrane (called, "PCL bilayer"); (ii) an electrospun PCL mat activated by air-plasma treatment and coated by layer-by-layer deposition with CTL and hyaluronic acid (called, "PCL coating"). To enrich the final products with antibacterial properties, the antibiotic rifampicin was then included in the basal PCL layer of both the PCL bilayer and PCL coating membranes, obtaining the so-called "Rif bilayer" and "Rif coating" matrices, which were all characterized by homogenous fibers free of any superficial defect.

The functionality of the membranes was consequently studied by initially analyzing their fluid retention ability. Indeed, it is known that the presence of exceeding exudates causes skin maceration, leading to inactivity of fibroblasts and extension of the inflammatory phase. This is then responsible for the self-perpetuation of the chronic wound, and thus complicates patient's treatment and increases its morbidity [59]. In a previous work, the hydrophobicity and the poor swelling behavior of untreated PCL membranes have been already characterized [36]. Here, both the plasma-treated PCL control membrane and the multilayer functionalized ones showed optimal swelling behavior; however, the fluid retention ability of the PCL coating mats was significantly lower than that of PCL and PCL bilayer membranes. This could be explained by the rapid hydration of the coating in aqueous environment, which shields the porosity of the underlying PCL network, with a consistent reduction in the ability to absorb fluids.

The water vapor permeability was assessed in parallel, as it is another essential requirement for a wound dressing, where the maintenance of a moist environment has been proven to favor the regeneration process, preventing scar formation [60]. The membranes tested here particularly provided an optimal moisture balance up to 72 h, in accordance with the mean frequency of dressing changes [61,62].

Thanks to the air-plasma treatment all types of matrices also displayed a fully wettable behavior. By investigating different types of fluids, the already known ability of rifampicin to interact with serum proteins was then demonstrated here, with an increase of membranes hydrophilicity even in the absence of the air-plasma treatment [63].

It should be noted that if, on the one hand, the interaction with the biological environment is essential for the success of a biomaterial, on the other hand the non-specific protein adsorption could potentially trigger a foreign body reaction, and thus impair the function and biocompatibility of the biomaterial [64]. According to the Berg's limit, a contact angle $\theta < 65°$ could avoid the non-specific interaction but this parameter does not consider the adsorption processes at the nanometer scale. On this level, Whitesides and coworkers found the so called "Whiteside rules", determining that the non-specific adsorption could be regulated by: (i) the presence of a hydrophilic surface; (ii) the presence of hydrogen bond acceptors; (iii) the absence of hydrogen bond donors; (iv) the absence of net charge [65,66]. Basing on these considerations, the use of strongly hydrophilic polymeric coatings could satisfy many of these rules. Thus, in the specific case of the multilayer matrices here synthetized, the non-specific protein adsorption should be avoided. The change in the biomaterial surface properties is even confirmed by the surface free energy studies carried out with the Owens−Wendt method, which revealed an increase in the polar component of the air-plasma treated mats as well as on the not treated PCL/Rif samples exposed to serum proteins, thus confirming the surface modification occurred [40,67].

Once assessed the surface properties of the multilayer membranes, their stability was characterized both in terms of polysaccharide and

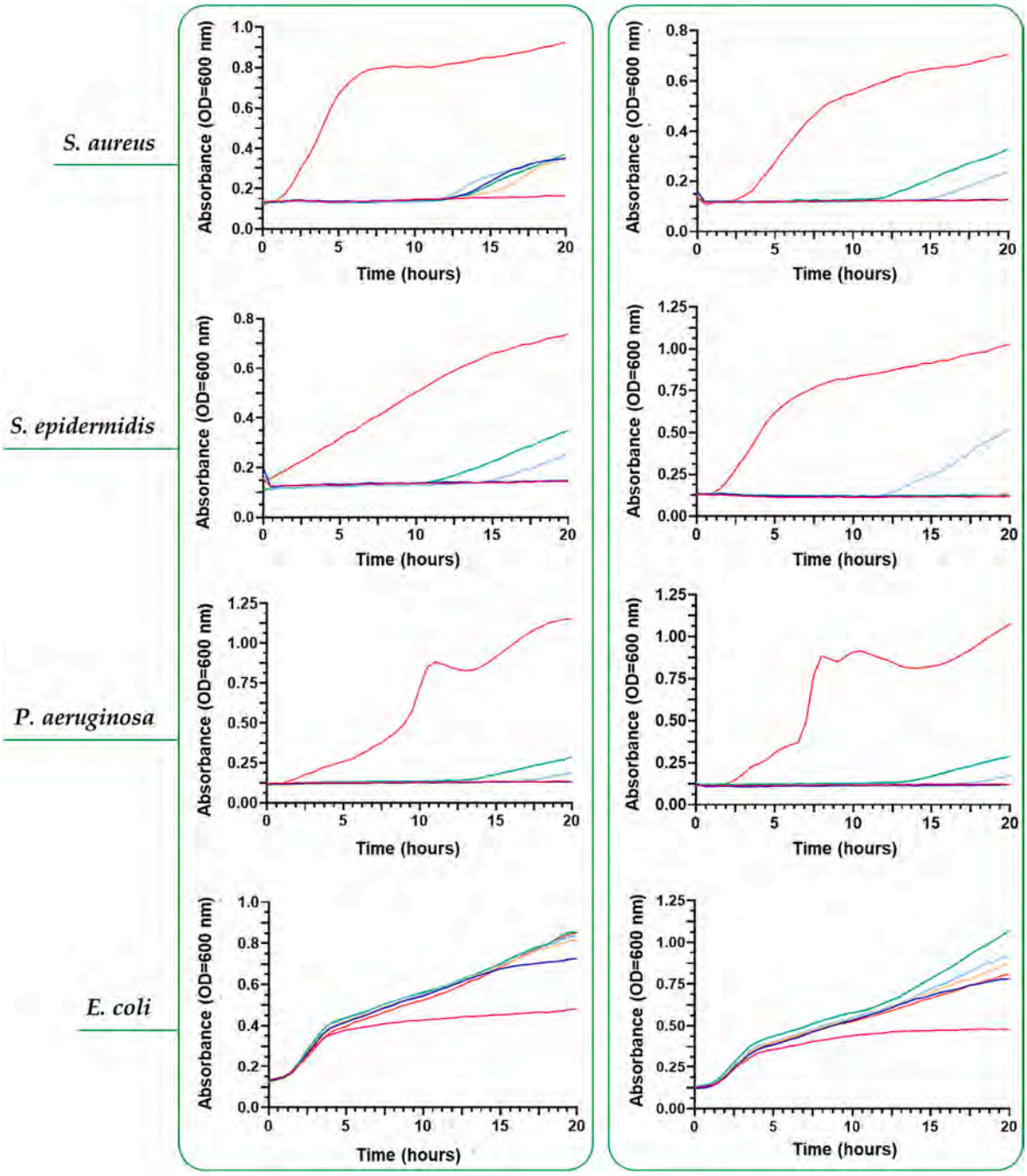

Fig. 13. Membrane antibacterial effect. Bacterial growth inhibition curves of the (left) Rif coating and (right) Rif bilayer membranes in the presence of four bacterial strains, that are *Staphylococcus aureus*, *Staphylococcus epidermidis*, *Pseudomonas aeruginosa*, and *Escherichia coli*. The red line indicates the control without antibiotic. Then, different rifampicin concentrations were tested: 5 μg/mL (pink line), 2.5 μg/mL (blue line), 1.25 μg/mL (yellow line), 0.625 μg/mL (light blue line), 0.3125 μg/mL (green line). $N = 2$.

rifampicin release. In the first case, an immediate dissolution of the polysaccharides from the PCL bilayer mats was observed, due to their high hydrophilicity in a non-crosslinked state combined with the typical high surface area of the nanofibrous architecture [68].

On the other hand, in the case of the PCL coating a burst release of the hyaluronic acid was registered, with a ≈ 84 % of release in 24 h; whereas the CTL coating was more stable and released slowly over time, reaching a ≈ 25 % of release after 24 h. This can be explained by the fact that the CTL is closely interconnected with the underlying activated PCL network and is thus retained on the structure. The hyaluronic acid constitutes, for its part, the outer unsteady layer of the coating, which is only weakly connected by electrostatic interactions between the residue charges on the two polymers and is therefore immediately available in the medium. Translating in the clinical practice, in both cases the outer PCL fibrous layer can protect the damaged site from external injuries, absorb the exudate, and favor the gaseous exchanges throughout the wound; meanwhile, the PCL bilayer could be useful for an immediate availability of the polysaccharides (which is particularly beneficial for wound dressings that need to be frequently changed), whilst the PCL coating membranes could serve for longer treatment times or as skin substitutes [69].

Similarly, the release of the loaded rifampicin was evaluated by

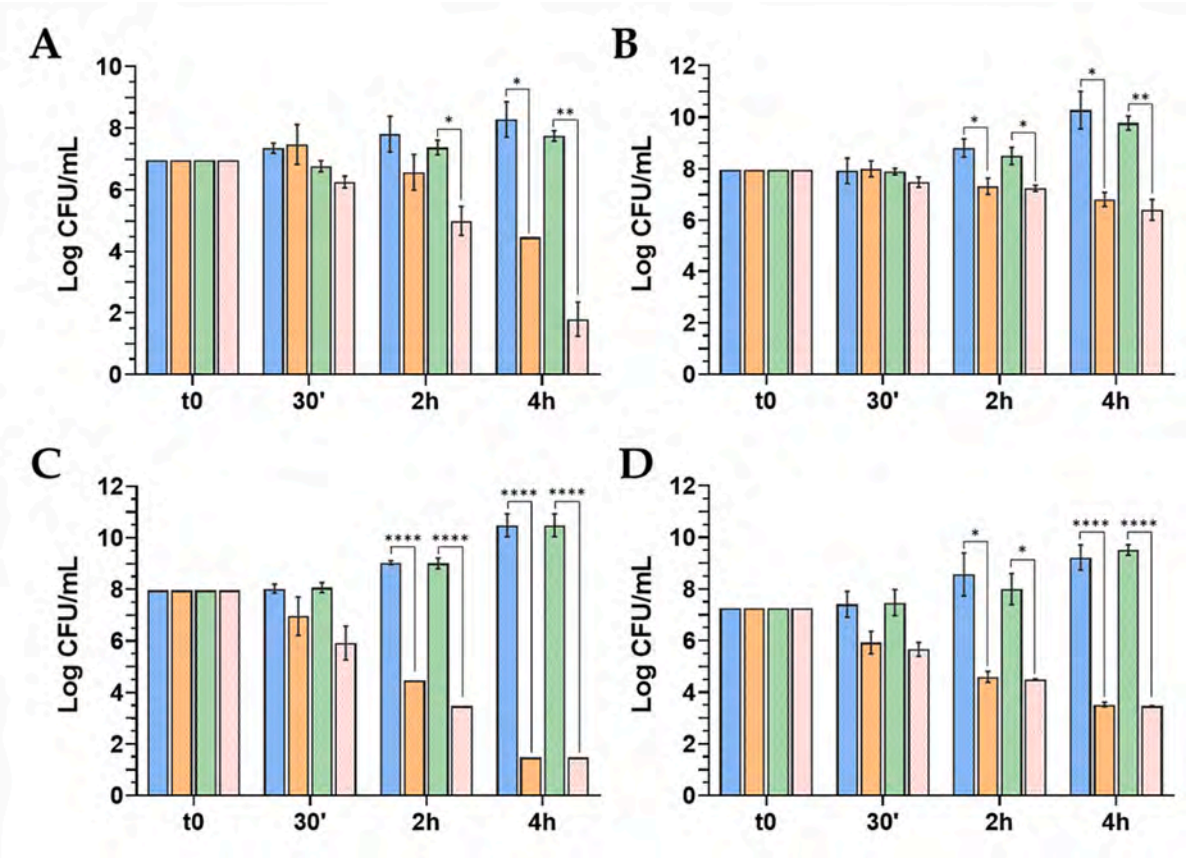

Fig. 14. Membranes bactericidal activity. Bactericidal activity of the rifampicin-loaded matrices over time, tested towards (A) *Staphylococcus aureus*, (B) *Escherichia coli*, (C) *Staphylococcus epidermidis*, and (D) *Pseudomonas aeruginosa*. The Rif coating and Rif bilayer samples are represented in the orange and light pink bars, respectively. The controls of PCL coating and PCL bilayer are indicated as blue and green bars, respectively. The statistical analysis was performed with ANOVA test, applying Bonferroni's correction. Statistically significant differences are indicated with asterisks (*). **** = $p < 0.0001$. $N = 4$.

comparing both untreated and plasma-treated membranes. Surprisingly, although all the matrices differ only for the polysaccharide deposition method and retain the same basal PCL/Rif layer, a higher rifampicin release was found in the case of the Rif bilayer. It was hypothesized, and then experimentally confirmed, that the immediate dissolution of the polysaccharides in the PBS medium increases the local salt concentration [70] thus shifting the release dissolution equilibrium towards the medium and driving the rifampicin out of the membrane. On the contrary, in the case of the PCL coating, the antibiotic is partially solubilized and trapped within the first coating layer, reducing the percentage of release over time. The release of drugs from electrospun mats then depends on diffusive processes from the nanofibrous mesh as well as from polymer degradation and drug dissolution [71]. Hence, the rifampicin is released here as free antibiotic from the multilayer matrices, and its mechanism of action is the same in all cases; the difference between Rif bilayer and Rif coating membranes rather lies in the release kinetic of the drug. It should be highlighted here that the dissolution of the rifampicin and its incorporation within the PCL mesh converts its crystallographic state into an amorphous one (as demonstrated by the XRD analysis), a factor that increases its bioavailability [72].

After characterizing their physicochemical properties, the biocompatibility of the membranes loaded or not with rifampicin was assessed using human dermal fibroblasts as cellular model. In no case was cell proliferation affected by the presence of the biomaterial, with a similar trend between all the types of treatments, which were comparable to the controls of untreated fibroblasts. It should be outlined that the wound healing process requires the dermal fibroblasts proliferation and migration towards the wound bed to reconstruct the ECM, promote granulation tissue formation, offer a support for inflammatory cell migration, and secrete cytokines, chemokines, and growth factors which guide cell response and survival in the wound site [73]. In this perspective, the bioactivity of both the PCL coating and PCL bilayer membranes was tested on human dermal fibroblasts through a wound healing assay, which mimics a wound *in vitro* thanks to the realization of a cellular gap ("scratch"), whose closure is measured over time. Both types of polysaccharide-based matrices revealed their bioactivity, inducing a significantly fast scratch closure already at the earlier timepoints. Even after 24 h, the scratch was still partially visible in the controls, whereas the wound was completely closed in the presence of the polysaccharides. On the other hand, no significant differences were detected between the PCL coating and PCL bilayer mats. In the future, the molecular processes responsible for the regenerative potential of the polysaccharides here employed will be thoroughly investigated.

Finally, given the urgent need for devices that can also counteract and prevent wound infections, the antibacterial efficacy of the rifampicin released from the antibiotic-loaded matrices was tested against four bacterial strains commonly infecting the wound site, namely the two Gram-positives *Staphylococcus aureus* and *Staphylococcus epidermidis* and the two Gram-negatives *Escherichia coli* and *Pseudomonas aeruginosa* [74–77]. The inhibitory activity was first assessed, by exposing the bacteria to rifampicin extracts obtained from the Rif coating and Rif bilayer membranes. Both in the case of Rif bilayer and Rif coating membranes, the antibiotic showed its efficacy in inhibiting Gram-positives and *Pseudomonas aeruginosa* growth. However, the same efficacy was not detected in the presence of *Escherichia coli*, which was resistant also at the higher drug concentration analyzed. Perhaps, the *Escherichia coli* strain adopted developed resistance to rifampicin thanks to a mutation in the β subunit of the bacterial RNA polymerase, as

systematically discussed by Goldstein [78]. Based on these findings, the bactericidal activity of rifampicin was tested in the presence of the four bacterial strains, this time using a more sensitive *Escherichia coli* strain. The released antibiotic proved its bactericidal activity over time towards all the bacteria tested, with *Staphylococcus epidermidis* being the most sensitive to rifampicin and *Escherichia coli* the less sensitive, which is consistent with the studied inhibitory activity. Further studies will investigate the loading of combined antibiotic drugs on the final product to achieve a higher antibacterial efficacy.

In synthesis, the multi-layered matrices described here could be of great advantage in wound treatment because: (i) they are easy to handle; (ii) they have suitable physicochemical properties; (iii) they are able to locally deliver bioactive polysaccharides; (iv) they can be easily functionalized with bioactive, anti-inflammatory, or antibacterial moieties to reach the final goal of optimal wound closure. Undoubtedly, some challenges and limitations are related to this work. On the one hand, the storage stability of the obtained matrices in environmental conditions should be ameliorated; on the other hand, further characterization is needed about their biological safety and bioactivity. Finally, the testing *in vivo* of animal models will be fundamental to predict the real performance of the final biomaterial.

5. Conclusions

Multilayer electrospun matrices with or without rifampicin were here prepared for the care of chronic wounds, by using two preparation methods: (i) sequential electrospinning of PCL and polysaccharides (namely, hyaluronic acid and CTL) to obtain a fully electrospun bilayer structure (the PCL bilayer), (ii) layer-by-layer deposition of CTL and hyaluronic acid on an electrospun PCL matrix (the PCL coating). The obtained devices exhibited optimal morphology given by defect-free and randomly oriented fibers. They also displayed suitable and physicochemical properties, thanks to their great fluid retention ability (3426 ± 492 % and 1435 ± 251 % for the PCL bilayer and PCL coating mats, respectively), water vapor permeability (160 ± 0.78 g/m^{2}h and 170 ± 12 g/m^{2}h in the case of the PCL bilayer and PCL coating meshes, respectively), and wettability (being totally wettable in the presence of various types of fluids, from water to cell culture medium). On the other hand, the different incorporation of polysaccharides and subsequent release of them opened two possible applications, namely wound dressings in the case of the fast-releasing PCL bilayer (with all the polysaccharides being released immediately) and skin substitutes in the case of the slow-releasing PCL coating (with only ≈25 % CTL being released after 24 h). All the membranes showed good biocompatibility in the presence of human dermal fibroblasts with the polysaccharides released from the multilayer matrices also exerting a bioactive activity. A wound healing assay on human dermal fibroblasts revealed, in fact, the ability of the polysaccharide-endowed matrices to faster heal the scratch (completely closed in 24 h) with respect to the controls. On the other hand, the released antibiotic displayed its bactericidal activity against *Staphylococcus aureus*, *Staphylococcus epidermidis*, and *Pseudomonas aeruginosa*, being less effective in the case of *Escherichia coli*. In the future, the synergistic activity of hyaluronic acid and CTL in inducing wound closure and tissue regeneration should be investigated *in vitro* and *in vivo* along with the use of animal models of chronic wounds.

Aknowledgments

The authors thanks Professor Ivan Donati for supplying the labeled polysaccharides (namely, CTL-FITC and HA-CF640R) and Professor Davide Lenaz for its help in performing the XRD analysis.

Funding sources

This research did not receive any specific grant from funding agencies in the public, commercial, or not-for-profit sectors.

CRediT authorship contribution statement

Martina Gruppuso: Conceptualization, Data curation, Investigation, Formal analysis, Writing – original draft. **Gianluca Turco:** Formal analysis, Writing – review & editing, Supervision. **Eleonora Marsich:** Formal analysis, Writing – review & editing, Supervision. **Davide Porrelli:** Conceptualization, Data curation, Investigation, Formal analysis, Writing – original draft, Supervision.

Declaration of competing interest

The authors declare the following financial interests/personal relationships which may be considered as potential competing interests: The authors Gianluca Turco and Eleonora Marsich declare to be shares holders of the company BiopoLife.

Data availability

Data will be made available on request.

Appendix A. Supplementary data

Dimensional analysis of nanofibers diameters; contact angle and surface energies analyses; images of the wound healing assay on human dermal fibroblasts, monitored at different timepoints and under different types of treatment. Supplementary data to this article can be found online at https://doi.org/10.1016/j.bioadv.2023.213613.

References

[1] Q. Chen, J. Wu, Y. Liu, Y. Li, C. Zhang, W. Qi, K.W.K. Yeung, T.M. Wong, X. Zhao, H. Pan, Electrospun chitosan/PVA/bioglass nanofibrous membrane with spatially designed structure for accelerating chronic wound healing, Mater. Sci. Eng. C. 105 (2019), 110083, https://doi.org/10.1016/j.msec.2019.110083.

[2] S. Baghersad, S. Hajir Bahrami, M.R. Mohammadi, M.R.M. Mojtahedi, P.B. Milan, Development of biodegradable electrospun gelatin/aloe-vera/poly(ε-caprolactone) hybrid nanofibrous scaffold for application as skin substitutes, Mater. Sci. Eng. C. 93 (2018) 367–379, https://doi.org/10.1016/j.msec.2018.08.020.

[3] Y. Yang, Y. Du, J. Zhang, H. Zhang, B. Guo, Structural and functional design of electrospun nanofibers for hemostasis and wound healing, Adv. Fiber Mater. 4 (2022) 1027–1057, https://doi.org/10.1007/s42765-022-00178-z.

[4] X. Zhang, R. Lv, L. Chen, R. Sun, Y. Zhang, R. Sheng, T. Du, Y. Li, Y. Qi, A multifunctional Janus electrospun nanofiber dressing with biofluid draining, monitoring, and antibacterial properties for wound healing, ACS Appl. Mater. Interfaces 14 (2022) 12984–13000, https://doi.org/10.1021/acsami.1c22629.

[5] A.D. Juncos Bombin, N.J. Dunne, H.O. Mccarthy, Electrospinning of natural polymers for the production of nanofibres for wound healing applications, Mater. Sci. Eng. C. 114 (2020), 110994, https://doi.org/10.1016/j.msec.2020.110994.

[6] P. Chandika, G.-W. Oh, S.-Y. Heo, S.-C. Kim, T.-H. Kim, M.-S. Kim, W.-K. Jung, Electrospun porous bilayer nano-fibrous fish collagen/PCL bio-composite scaffolds with covalently cross-linked chitooligosaccharides for full-thickness wound-healing applications, Mater. Sci. Eng. C. 121 (2021), 111871, https://doi.org/10.1016/j.msec.2021.111871.

[7] A. Eskandarinia, A. Kefayat, M. Gharakhloo, M. Agheb, D. Khodabakhshi, M. Khorshidi, V. Sheikhmoradi, M. Rafienia, H. Salehi, A propolis enriched polyurethane-hyaluronic acid nanofibrous wound dressing with remarkable antibacterial and wound healing activities, Int. J. Biol. Macromol. 149 (2020) 467–476, https://doi.org/10.1016/j.ijbiomac.2020.01.255.

[8] Q. Yang, Z. Xie, J. Hu, Y. Liu, Hyaluronic acid nanofiber mats loaded with antimicrobial peptide towards wound dressing applications, Mater. Sci. Eng. C. 128 (2021), 112319, https://doi.org/10.1016/j.msec.2021.112319.

[9] L. Zhang, U. D'Amora, A. Ronca, Y. Li, X. Mo, F. Zhou, M. Yuan, L. Ambrosio, J. Wu, M. Grazia Raucci, In vitro and in vivo biocompatibility and inflammation response of methacrylated and maleated hyaluronic acid for wound healing, RSC Adv. 10 (2020) 32183–32192, https://doi.org/10.1039/D0RA06025A.

[10] J. Xia, H. Zhang, F. Yu, Y. Pei, X. Luo, Superclear, porous cellulose membranes with chitosan-coated nanofibers for visualized cutaneous wound healing dressing, ACS Appl. Mater. Interfaces 12 (2020) 24370–24379, https://doi.org/10.1021/acsami.0c05604.

[11] P. Marcon, E. Marsich, A. Vetere, P. Mozetic, C. Campa, I. Donati, F. Vittur, A. Gamini, S. Paoletti, The role of Galectin-1 in the interaction between chondrocytes and a lactose-modified chitosan, Biomaterials 26 (2005) 4975–4984, https://doi.org/10.1016/j.biomaterials.2005.01.044.

[12] R. Augustine, S. Rehman, R. Ahmed, A. Zahid, M. Shari, M. Falahati, A. Hasan, Electrospun chitosan membranes containing bioactive and therapeutic agents for enhanced wound healing, Int. J. Biol. Macromol. 156 (2020) 153–170, https://doi.org/10.1016/j.ijbiomac.2020.03.207.

[13] D. Porrelli, M. Gruppuso, F. Vecchies, E. Marsich, G. Turco, Alginate bone scaffolds coated with a bioactive lactose modified chitosan for human dental pulp stem cells proliferation and differentiation, Carbohydr. Polym. 273 (2021), 118610, https://doi.org/10.1016/j.carbpol.2021.118610.
[14] A. Donato, E. Belluzzi, E. Mattiuzzo, R. Venerando, M. Cadamuro, P. Ruggieri, V. Vindigni, P. Brun, Anti-inflammatory and pro-regenerative effects of hyaluronan-Chitlac mixture in human dermal fibroblasts: a skin ageing perspective, Polymers 14 (2022) 1817, https://doi.org/10.3390/polym14091817.
[15] M. Gruppuso, G. Turco, E. Marsich, D. Porrelli, Polymeric wound dressings, an insight into polysaccharide-based electrospun membranes, Appl. Mater. Today 24 (2021), 101148, https://doi.org/10.1016/j.apmt.2021.101148.
[16] X. Zhao, S. Chen, Z. Lin, C. Du, Reactive electrospinning of composite nanofibers of carboxymethyl chitosan cross-linked by alginate dialdehyde with the aid of polyethylene oxide, Carbohydr. Polym. 148 (2016) 98–106, https://doi.org/10.1016/j.carbpol.2016.04.051.
[17] D.P. Facchi, S.P. Facchi, P.R. Souza, E.G. Bonafé, K.C. Popat, M.J. Kipper, A. F. Martins, Composite filter with antimicrobial and anti-adhesive properties based on electrospun poly(butylene adipate-co-terephthalate)/poly(acid lactic)/tween 20 fibers associated with silver nanoparticles, J. Membr. Sci. 650 (2022), 120426, https://doi.org/10.1016/j.memsci.2022.120426.
[18] E.J. Dierings de Souza, D.H. Kringel, A.R. Guerra Dias, E. da Rosa Zavareze, Polysaccharides as wall material for the encapsulation of essential oils by electrospun technique, Carbohydr. Polym. 265 (2021), 118068, https://doi.org/10.1016/j.carbpol.2021.118068.
[19] H. Xu, F. Zhang, M. Wang, H. Lv, D.-G. Yu, X. Liu, H. Shen, Electrospun hierarchical structural films for effective wound healing, Biomater. Adv. 136 (2022), 212795, https://doi.org/10.1016/j.bioadv.2022.212795.
[20] A.Z. Bazmandeh, E. Mirzaei, Y. Ghasemi, M.A.J. Kouhbanani, Hyaluronic acid coated electrospun chitosan-based nanofibers prepared by simultaneous stabilizing and coating, Int. J. Biol. Macromol. 138 (2019) 403–411, https://doi.org/10.1016/j.ijbiomac.2019.07.107.
[21] A. Jafari, A. Amirsadeghi, S. Hassanajili, N. Azarpira, Bioactive antibacterial bilayer PCL/gelatin nanofibrous scaffold promotes full-thickness wound healing, Int. J. Pharm. 583 (2020), 119413, https://doi.org/10.1016/j.ijpharm.2020.119413.
[22] A.A. Hassan, H.A. Radwan, S.A. Abdelaal, N.S. Al-Radadi, M.K. Ahmed, K. R. Shoueir, M.A. Hady, Polycaprolactone based electrospun matrices loaded with Ag/hydroxyapatite as wound dressings: morphology, cell adhesion, and antibacterial activity, Int. J. Pharm. 593 (2021), 120143, https://doi.org/10.1016/j.ijpharm.2020.120143.
[23] J.M. Anaya Mancipe, L.C. Boldrini Pereira, P.G. de Miranda Borchio, M.L. Dias, R. M. da Silva Moreira Thiré, Novel polycaprolactone (PCL)-type I collagen core-shell electrospun nanofibers for wound healing applications, J. Biomed. Mater. Res. Part B Appl. Biomater. (2022), https://doi.org/10.1002/jbm.b.35156 (n/a).
[24] Y. Qi, C. Wang, Q. Wang, F. Zhou, T. Li, B. Wang, W. Su, D. Shang, S. Wu, A simple, quick, and cost-effective strategy to fabricate polycaprolactone/silk fibroin nanofiber yarns for biotextile-based tissue scaffold application, Eur. Polym. J. 186 (2023), 111863, https://doi.org/10.1016/j.eurpolymj.2023.111863.
[25] S. Wu, W. Zhao, M. Sun, P. He, H. Lv, Q. Wang, S. Zhang, Q. Wu, P. Ling, S. Chen, J. Ma, Novel bi-layered dressing patches constructed with radially-oriented nanofibrous pattern and herbal compound-loaded hydrogel for accelerated diabetic wound healing, Appl. Mater. Today 28 (2022), 101542, https://doi.org/10.1016/j.apmt.2022.101542.
[26] H.R. Bakhsheshi-Rad, Z. Hadisi, A.F. Ismail, M. Aziz, M. Akbari, F. Berto, X. B. Chen, In vitro and in vivo evaluation of chitosan-alginate/gentamicin wound dressing nanofibrous with high antibacterial performance, Polym. Test. 82 (2020), 106298, https://doi.org/10.1016/j.polymertesting.2019.106298.
[27] H.R. Bakhsheshi-Rad, A. Fauzi, M. Aziz, M. Akbari, Z. Hadisi, M. Omidi, X. Chen, Development of the PVA/CS nano fibers containing silk protein sericin as a wound dressing: in vitro and in vivo assessment, Int. J. Biol. Macromol. 149 (2020) 513–521, https://doi.org/10.1016/j.ijbiomac.2020.01.139.
[28] G. Brandis, D. Hughes, Genetic characterization of compensatory evolution in strains carrying rpoB Ser531Leu, the rifampicin resistance mutation most frequently found in clinical isolates, J. Antimicrob. Chemother. 68 (2013) 2493–2497, https://doi.org/10.1093/jac/dkt224.
[29] A. Singh, S. Grover, S. Sinha, M. Das, P. Somvanshi, A. Grover, Mechanistic principles behind molecular mechanism of rifampicin resistance in mutant RNA polymerase beta subunit of mycobacterium tuberculosis, J. Cell. Biochem. 118 (2017) 4594–4606, https://doi.org/10.1002/jcb.26124.
[30] M. Grobbelaar, G.E. Louw, S.L. Sampson, P.D. van Helden, P.R. Donald, R. M. Warren, Evolution of rifampicin treatment for tuberculosis, Infect. Genet. Evol. 74 (2019), 103937, https://doi.org/10.1016/j.meegid.2019.103937.
[31] A.S. Kranthi Kiran, A. Kizhakeyil, R. Ramalingam, N.K. Verma, R. Lakshminarayanan, T.S.S. Kumar, M. Doble, S. Ramakrishna, Drug loaded electrospun polymer/ceramic composite nanofibrous coatings on titanium for implant related infections, Ceram. 45 (2019) 18710–18720, https://doi.org/10.1016/j.ceramint.2019.06.097.
[32] A. Walduck, P. Sangwan, Q. Anh Vo, J. Ratcliffe, J. White, B.W. Muir, N. Tran, Treatment of Staphylococcus aureus skin infection in vivo using rifampicin loaded lipid nanoparticles, RSC Adv. 10 (2020) 33608–33619, https://doi.org/10.1039/D0RA06120D.
[33] C.M.J. Drapeau, E. Grilli, N. Petrosillo, Rifampicin combined regimens for gram-negative infections: data from the literature, Int. J. Antimicrob. Agents 35 (2010) 39–44, https://doi.org/10.1016/j.ijantimicag.2009.08.011.
[34] F. Furlani, P. Sacco, E. Marsich, I. Donati, S. Paoletti, Highly monodisperse colloidal coacervates based on a bioactive lactose-modified chitosan: from synthesis to characterization, Carbohydr. Polym. 174 (2017) 360–368, https://doi.org/10.1016/j.carbpol.2017.06.097.
[35] D. Porrelli, M. Mardirossian, L. Musciacchio, M. Pacor, F. Berton, M. Crosera, G. Turco, Antibacterial electrospun polycaprolactone membranes coated with polysaccharides and silver nanoparticles for guided bone and tissue regeneration, ACS Appl. Mater. Interfaces 13 (2021) 17255–17267, https://doi.org/10.1021/acsami.1c01016.
[36] M. Gruppuso, F. Iorio, G. Turco, E. Marsich, D. Porrelli, Hyaluronic acid/lactose-modified chitosan electrospun wound dressings – crosslinking and stability criticalities, Carbohydr. Polym. 288 (2022), 119375, https://doi.org/10.1016/j.carbpol.2022.119375.
[37] M. Gruppuso, B. Guagnini, L. Musciacchio, F. Bellemo, G. Turco, D. Porrelli, Tuning the drug release from antibacterial polycaprolactone/rifampicin-based core–shell electrospun membranes: a proof of concept, ACS Appl. Mater. Interfaces (2022), https://doi.org/10.1021/acsami.2c04849.
[38] J. Schindelin, I. Arganda-Carreras, E. Frise, V. Kaynig, M. Longair, T. Pietzsch, S. Preibisch, C. Rueden, S. Saalfeld, B. Schmid, J.-Y. Tinevez, D.J. White, V. Hartenstein, K. Eliceiri, P. Tomancak, A. Cardona, Fiji: an open-source platform for biological-image analysis, Nat. Methods 9 (2012) 676–682, https://doi.org/10.1038/nmeth.2019.
[39] L. Tarusha, S. Paoletti, A. Travan, E. Marsich, Alginate membranes loaded with hyaluronic acid and silver nanoparticles to foster tissue healing and to control bacterial contamination of non-healing wounds, J. Mater. Sci. Mater. Med. 29 (2018) 22, https://doi.org/10.1007/s10856-018-6027-7.
[40] D.K. Owens, Estimation of the surface free energy of polymers, J. Appl. Polym. Sci. 13 (1969) 1741–1747, https://doi.org/10.1002/app.1969.070130815.
[41] Z. Ren, G. Chen, Z. Wei, L. Sang, M. Qi, Hemocompatibility evaluation of polyurethane film with surface-grafted poly(ethylene glycol) and carboxymethyl-chitosan, J. Appl. Polym. Sci. 127 (2013) 308–315, https://doi.org/10.1002/app.37885.
[42] L.A. Can-Herrera, A. Ávila-Ortega, S. de la Rosa-García, A.I. Oliva, J.V. Cauich-Rodríguez, J.M. Cervantes-Uc, Surface modification of electrospun polycaprolactone microfibers by air plasma treatment: effect of plasma power and treatment time, Eur. Polym. J. 84 (2016) 502–513, https://doi.org/10.1016/j.eurpolymj.2016.09.060.
[43] P. Sacco, E. Decleva, F. Tentor, R. Menegazzi, M. Borgogna, S. Paoletti, K. A. Kristiansen, K.M. Vårum, E. Marsich, Butyrate-loaded chitosan/hyaluronan nanoparticles: a suitable tool for sustained inhibition of ROS release by activated neutrophils, Macromol. Biosci. 17 (2017) 1700214, https://doi.org/10.1002/mabi.201700214.
[44] M. He, J. Xue, H. Geng, H. Gu, D. Chen, R. Shi, L. Zhang, Fibrous guided tissue regeneration membrane loaded with anti-inflammatory agent prepared by coaxial electrospinning for the purpose of controlled release, Appl. Surf. Sci. 335 (2015) 121–129, https://doi.org/10.1016/j.apsusc.2015.02.037.
[45] C. Yuan, D. Zhang, Y. Tang, Z. Guo, K. Lin, Y. Yu, J. Li, Q. Cai, Fibrous dressing containing bioactive glass with combined chemotherapy and wound healing promotion for post-surgical treatment of melanoma, Biomater. Adv. 149 (2023), 213387, https://doi.org/10.1016/j.bioadv.2023.213387.
[46] Z. Wang, X. Song, Y. Cui, K. Cheng, X. Tian, M. Dong, L. Liu, Silk fibroin H-fibroin/poly(ε-caprolactone) core-shell nanofibers with enhanced mechanical property and long-term drug release, J. Colloid Interface Sci. 593 (2021) 142–151, https://doi.org/10.1016/j.jcis.2021.02.099.
[47] A. Henderson, D.L. Paterson, M.D. Chatfield, P.A. Tambyah, D.C. Lye, P.P. De, R.T. P. Lin, K.L. Chew, M. Yin, T.H. Lee, M. Yilmaz, R. Cakmak, T.H. Alenazi, Y. M. Arabi, M. Falcone, M. Bassetti, E. Righi, B.A. Rogers, S.S. Kanj, H. Bhally, J. Iredell, M. Mendelson, T.H. Boyles, D.F.M. Looke, N.J. Runnegar, S. Miyakis, G. Walls, M.A.I. Khamis, A. Zikri, A. Crowe, P.R. Ingram, N. Daneman, P. Griffin, E. Athan, L. Roberts, S.A. Beatson, A.Y. Peleg, K. Cottrell, M.J. Bauer, E. Tan, K. Chaw, G.R. Nimmo, T. Harris-Brown, P.N.A. Harris, MERINO Trial Investigators and the Australasian Society for Infectious Disease Clinical Research Network (ASID-CRN)[Corporate Author], Association between minimum inhibitory concentration, beta-lactamase genes and mortality for patients treated with Piperacillin/Tazobactam or Meropenem from the MERINO study, Clin. Infect. Dis. 73 (2021) e3842–e3850, https://doi.org/10.1093/cid/ciaa1479.
[48] B. Kowalska-Krochmal, R. Dudek-Wicher, The minimum inhibitory concentration of sntibiotics: methods, interpretation, clinical relevance, Pathogens 10 (2021) 165, https://doi.org/10.3390/pathogens10020165.
[49] L. Musciacchio, M. Mardirossian, B. Guagnini, A. Raffini, M. Rizzo, C. Trombetta, G. Liguori, G. Turco, D. Porrelli, Rifampicin-loaded electrospun polycaprolactone membranes: characterization of stability, antibacterial effects and urotheliocytes proliferation, Mater. Des. 224 (2022), 111286, https://doi.org/10.1016/j.matdes.2022.111286.
[50] I.T. Zedan, E.M. El-Menyawy, A.M. Mansour, Physical characterizations of 3-(4-methyl piperazinylimino methyl) rifampicin films for photodiode applications, Silicon 11 (2019) 1693–1699, https://doi.org/10.1007/s12633-018-9989-7.
[51] J. Singh, P.M. Pandey, T. Kaur, N. Singh, Surface characterization of polycaprolactone and carbonyl iron powder composite fabricated by solvent cast 3D printing for tissue engineering, Polym. Compos. 42 (2021) 865–871, https://doi.org/10.1002/pc.25871.
[52] R.B. Trinca, C.B. Westin, J.A.F. da Silva, Â.M. Moraes, Electrospun multilayer chitosan scaffolds as potential wound dressings for skin lesions, Eur. Polym. J. 88 (2017) 161–170, https://doi.org/10.1016/j.eurpolymj.2017.01.021.
[53] G.-W. Oh, S.Y. Nam, S.-J. Heo, D.-H. Kang, W.-K. Jung, Characterization of ionic cross-linked composite foams with different blend ratios of alginate/pectin on the synergistic effects for wound dressing application, Int. J. Biol. Macromol. 156 (2020) 1565–1573, https://doi.org/10.1016/j.ijbiomac.2019.11.206.

[54] M.U.A. Khan, M.A. Raza, S.I.A. Razak, M.R. Abdul Kadir, A. Haider, S.A. Shah, A. H. Mohd Yusof, S. Haider, I. Shakir, S. Aftab, Novel functional antimicrobial and biocompatible arabinoxylan/guar gum hydrogel for skin wound dressing applications, J. Tissue Eng. Regen. Med. 14 (2020) 1488–1501, https://doi.org/10.1002/term.3115.
[55] M. Minsart, S. Van Vlierberghe, P. Dubruel, A. Mignon, Commercial wound dressings for the treatment of exuding wounds: an in-depth physico-chemical comparative study, Burns Trauma 10 (2022) tkac024, https://doi.org/10.1093/burnst/tkac024.
[56] P.T.S. Kumar, S. Abhilash, K. Manzoor, S.V. Nair, H. Tamura, R. Jayakumar, Preparation and characterization of novel β-chitin/nanosilver composite scaffolds for wound dressing applications, Carbohydr. Polym. 80 (2010) 761–767, https://doi.org/10.1016/j.carbpol.2009.12.024.
[57] M. Bagheri, M. Validi, A. Gholipour, P. Makvandi, E. Sharifi, Chitosan nanofiber biocomposites for potential wound healing applications: antioxidant activity with synergic antibacterial effect, Bioeng. Transl. Med. 7 (2022), https://doi.org/10.1002/btm2.10254.
[58] G. Guan, S. Qizhuang Lv, Z. Liu, C. Jiang, W. Liao Zhou, 3D-bioprinted peptide coupling patches for wound healing, Mater. Today Bio. 13 (2022), 100188, https://doi.org/10.1016/j.mtbio.2021.100188.
[59] Y. Li, Y. Zhang, Y. Wang, K. Yu, E. Hu, F. Lu, S. Shang, R. Xie, G. Lan, Regulating wound moisture for accelerated healing: a strategy for the continuous drainage of wound exudates by mimicking plant transpiration, Chem. Eng. J. 429 (2022), 131964, https://doi.org/10.1016/j.cej.2021.131964.
[60] G. Winter, Formation of the scab and the rate of epithelization of superficial wounds in the skin of the young domestic pig, Nature 193 (1962) 293–294, https://doi.org/10.1038/193293a0.
[61] C. Lindholm, R. Searle, Wound management for the 21st century: combining effectiveness and efficiency, Int. Wound J. 13 (2016) 5–15, https://doi.org/10.1111/iwj.12623.
[62] A. Resch, C. Staud, C. Radtke, Nanocellulose-based wound dressing for conservative wound management in children with second-degree burns, Int. Wound J. 18 (2021) 478–486, https://doi.org/10.1111/iwj.13548.
[63] G. Boman, V.A. Ringberger, Binding of rifampicin by human plasma proteins, Eur. J. Clin. Pharmacol. 7 (1974) 369–373, https://doi.org/10.1007/BF00558209.
[64] Q. Wei, T. Becherer, S. Angioletti-Uberti, J. Dzubiella, C. Wischke, A.T. Neffe, A. Lendlein, M. Ballauff, R. Haag, Protein interactions with polymer coatings and biomaterials, Angew. Chem. Int. Ed. 53 (2014) 8004–8031, https://doi.org/10.1002/anie.201400546.
[65] J.M. Berg, L.G.T. Eriksson, P.M. Claesson, K.G.N. Borve, Three-component Langmuir-Blodgett films with a controllable degree of polarity, Langmuir 10 (1994) 1225–1234, https://doi.org/10.1021/la00016a041.
[66] E. Ostuni, R.G. Chapman, R.E. Holmlin, S. Takayama, G.M. Whitesides, A survey of structure−property relationships of surfaces that resist the adsorption of protein, Langmuir 17 (2001) 5605–5620, https://doi.org/10.1021/la010384m.
[67] A. Rudawska, E. Jacniacka, Analysis for determining surface free energy uncertainty by the Owen–Wendt method, Int. J. Adhes. Adhes. 29 (2009) 451–457, https://doi.org/10.1016/j.ijadhadh.2008.09.008.
[68] X. Gao, R. Huang, Y. Jiao, T. Groth, W. Yang, C. Tu, H. Li, F. Gong, J. Chu, M. Zhao, Enhanced wound healing in diabetic mice by hyaluronan/chitosan multilayer-coated PLLA nanofibrous mats with sustained release of insulin, Appl. Surf. Sci. 576 (2022), 151825, https://doi.org/10.1016/j.apsusc.2021.151825.
[69] D. Chouhan, N. Thatikonda, L. Nilebäck, M. Widhe, M. Hedhammar, B.B. Mandal, Recombinant spider silk functionalized silkworm silk natrices as potential bioactive wound dressings and skin grafts, ACS Appl. Mater. Interfaces 10 (2018) 23560–23572, https://doi.org/10.1021/acsami.8b05853.
[70] K. Joanna, P. Michał, P. Anna, Osmotic properties of polysaccharides solutions, IntechOpen (2017), https://doi.org/10.5772/intechopen.69864.
[71] S.-F. Chou, D. Carson, K.A. Woodrow, Current strategies for sustaining drug release from electrospun nanofibers, J. Control. Release 220 (2015) 584–591, https://doi.org/10.1016/j.jconrel.2015.09.008.
[72] P. Khadka, S. Sinha, I.G. Tucker, J. Dummer, P.C. Hill, R. Katare, S.C. Das, Pharmacokinetics of rifampicin after repeated intra-tracheal administration of amorphous and crystalline powder formulations to Sprague Dawley rats, Eur. J. Pharm. Biopharm. 162 (2021) 1–11, https://doi.org/10.1016/j.ejpb.2021.02.011.
[73] R. Belvedere, N. Novizio, S. Morello, A. Petrella, The combination of mesoglycan and VEGF promotes skin wound repair by enhancing the activation of endothelial cells and fibroblasts and their cross-talk, Sci. Rep. 12 (2022) 11041, https://doi.org/10.1038/s41598-022-15227-1.
[74] M. Yokota, N. Häffner, M. Kassier, M. Brunner, S.M. Shambat, F. Brennecke, J. Schniering, E. Marques Maggio, O. Distler, A.S. Zinkernagel, B. Maurer, Staphylococcus aureus impairs dermal fibroblast functions with deleterious effects on wound healing, FASEB J. 35 (2021), e21695, https://doi.org/10.1096/fj.201902836R.
[75] M.M. Severn, A.R. Horswill, Staphylococcus epidermidis and its dual lifestyle in skin health and infection, Nat. Rev. Microbiol. (2022) 1–15, https://doi.org/10.1038/s41579-022-00780-3.
[76] A. Oliveira, J.C. Sousa, A.C. Silva, L.D.R. Melo, S. Sillankorva, Chestnut honey and bacteriophage application to control Pseudomonas aeruginosa and Escherichia coli biofilms: evaluation in an ex vivo wound model, Front. Microbiol. 9 (2018), https://doi.org/10.3389/fmicb.2018.01725.
[77] S. DeLeon, A. Clinton, H. Fowler, J. Everett, A.R. Horswill, K.P. Rumbaugh, Synergistic interactions of Pseudomonas aeruginosa and Staphylococcus aureus in an in vitro wound model, Infect. Immun. 82 (2014) 4718–4728, https://doi.org/10.1128/IAI.02198-14.
[78] B.P. Goldstein, Resistance to rifampicin: a review, J. Antibiot. 67 (2014) 625–630, https://doi.org/10.1038/ja.2014.107.

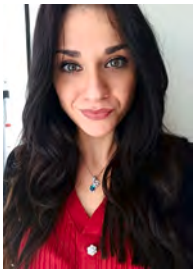

Martina Gruppuso holds a master's degree in Medical Biotechnology (curriculum Nanobiotechnology) (2019) and has recently achieved a PhD in Reproduction and Developmental Sciences at the University of Trieste. She is active in the biomaterial and tissue engineering fields, ranging from polymeric 3D-scaffolds, with a special focus on bone regeneration, to nanofibrous matrices. Her ongoing research activity is dedicated to the production of micro- and nano-structured electrospun membranes for wound dressing applications. She already first-authored two research papers and one literature review on electrospun devices for biomedical applications, published on highly impacted journals.

Gianluca Turco graduated in 2006 in Materials Engineering, then he did his PhD studying biomaterials, their characterization and interaction with cells. In October 2019 he became Associate Professor at the University of Trieste. His fields of investigation are related to tissue engineering and regenerative medicine. He is author or co-author of >60 papers published on international journals with impact factor. He is co-inventor of two patents in the field of materials for biomedical purposes. He is reviewer of several international journals in the fields of biomaterials, tissue engineering and regenerative medicine.

Eleonora Marsich is Associate Professor at the Department of Medicine of the University of Trieste. She has a Master's Degree in Molecular Biology and a PhD in Biochemistry. Her research activities are mainly focused on the study of materials based on natural or natural- derived polymers, on the synthesis and physical, chemical and biological characterization of modified polysaccharides and on the study of the molecular mechanisms underlying the interaction between cells/tissues and materials. She has authored >90 research papers in peer reviewed journals (H- index 27), 5 book chapters and 8 international patents.

Davide Porrelli. He is a Medical Biotechnologist graduated in 2012 at the university of Trieste. During his PhD in Nanotechnology he worked on polysaccharide-based biomaterials for bone and neural tissue regeneration. Since June 2016 he has been working as a post-doc researcher in the Dental Materials Laboratory of the Dental School in Trieste, on polymer-based biomaterials, and in the recent years he started to manage projects on bioactive and antibacterial electrospun biomaterials; he is now also an electron microscopy technician. He published several papers on international journals with impact factor, and he is a reviewer for international journals focused on biomaterials.